Vaccine Induction in Humans of Polyclonal HIV-1 Heterologous Neutralizing Antibodies

By

Wilton B. Williams[1,2,5,*&], S. Munir Alam[1,4,*&], Gilad Ofek[3,15,&], Nathaniel Erdmann[9,&], David Montefiori[1,2,&], Michael Seaman[12], Kshitij Wagh[14], Bette Korber[14], Robert J. Edwards[1,4], Katayoun Mansouri[1], Amanda Eaton[2], Derek W. Cain[1,4], Robert Parks[1], Maggie Barr[1], Mitchell Martin[1], Jongln Hwang[1], Andrew Foulger[1], Kara Anasti[1], Salam Sammour[1], Xiao Huang[1], Jared Lindenberger[1], Katarzyna Janowska[1], Aurelie Niyongabo[3], Benjamin M. Janus[3,15], Anagh Astavans[3], Christopher Fox[13], Ipsita Mohanty[1], Tyler Evangelous[1], Madison Berry[1], Helene Kirshner[1], Kevin Saunders[1,2,5,6], Kevin Wiehe[1,4], Kristen Cohen[7], M. Juliana McElrath[7], Lawrence Corey[7], Priyamvada Acharya[1,2,10], Stephen R. Walsh[8,*], Lindsey R. Baden[8,*] and Barton F. Haynes[1,4,5,11,*].

[1]Duke Human Vaccine Institute, Duke School of Medicine, Durham, NC 27710

[2]Department of Surgery, Duke School of Medicine, Durham, NC 27710

[3]Department of Cell Biology and Molecular Genetics, University of Maryland, College Park, MD 20742

[4]Department of Medicine, Duke School of Medicine, Durham, NC 27710

[5]Department of Immunology, Duke School of Medicine, Durham, NC 27710

[6]Department of Molecular Genetics and Microbiology, Duke School of Medicine, Durham, NC 27710

[7]Fred Hutchinson Cancer Research Center, Seattle WA 98109

[8]Brigham and Women's Hospital, Harvard Medical School, Boston MA 02115

[9]University of Alabama Medical Center, Birmingham AL 35223

[10]Department of Biochemistry, Duke School of Medicine, Durham, NC 27710

[11]Duke Global Health Institute, Duke School of Medicine, Durham, NC 27710

[12]Beth Israel Deaconess Medical Center, Harvard Medical School, Boston MA 02215

[13]Access to Access to Advanced Health Institute, Seattle WA, 98102

[14]Los Alamos National Laboratory, Los Alamos NM, 87545

[15]Institute for Bioscience and Biotechnology Research, University of Maryland, Rockville MD 20850

[&]These authors contributed equally to this work.

*Corresponding Authors: wilton.williams@duke.edu; munir.alam@duke.edu; barton.haynes@duke.edu; lbaden@bwh.harvard.edu; SWALSH@bwh.harvard.edu

Wilton Williams, Ph.D.
Associate Professor of Surgery
2 Genome Court
MSRBII Bldg. Room 4076
DUMC 103020
Duke University Medical Center
Durham, NC 27710
Ph: 919-660-1546
Fx: 919-684-5230
wilton.williams@duke.edu

S. Munir Alam
Professor in Medicine & Pathology
2 Genome Court
MSRBII Bldg. Room 3009
DUMC 103020
Duke University Medical Center
Durham, NC 27710
Ph: 919-668-6372
Fx: 919-684-5230

Lindsey R. Baden, MD
Professor, Harvard Medical School
Brigham and Women's Hospital
70 Francis St,
Boston, MA 02115
Phone: (617) 732-6801
lbaden@bwh.harvard.edu

Stephen R. Walsh, MD
Assistant Professor of Medicine
Harvard Medical School
Brigham and Women's Hospital
3 Blackfan Circle
Boston, MA 02115
Ph: 617-735-4548
swalsh@bwh.harvard.edu

Barton F. Haynes, M.D.
Director, Duke Human Vaccine Institute
Frederic M. Hanes Professor of Medicine
Professor of Immunology
2 Genome Court
MSRBII Bldg. Room 4090
DUMC 103020
Duke University Medical Center
Durham, NC 27710

Ph: 919-684-5279
Fx: 919-684-5230
barton.haynes@duke.edu

Abstract

A major roadblock to the development of a safe and effective HIV-1 vaccine has been the inability to induce broadly neutralizing antibodies (bnAbs) in humans. Potent HIV-1 bnAb induction is disfavored by both host and viral factors. A Phase I clinical trial was conducted with a peptide/liposome immunogen targeting the unmutated ancestor of a HIV-1 envelope gp41 membrane proximal external region (MPER) bnAb B cell lineage (NCT03934541). Here, we report vaccine induction of a polyclonal heterologous nAb response in humans of gp41 MPER bnAb precursor and intermediate lineage B cells, the most potent of which neutralized difficult-to-neutralize tier 2 HIV-1 strains. Thus, this study demonstrates a proof-of-concept for vaccine induction of heterologous HIV-1 neutralizing B cell responses in humans and provides hope that development of a preventive Ab-inducing HIV-1 vaccine may ultimately be possible.

Summary paragraph

A major roadblock to the development of a safe and effective HIV-1 vaccine has been the inability to induce broadly neutralizing antibodies (bnAbs) in humans (*1, 2*). However, potent HIV-1 bnAb induction by vaccines is disfavored by both host immune tolerance and virus envelope (Env) structural constraints (*3, 4*). While bnAbs develop in HIV-1-infected individuals, they do so rarely and only after years of infection (*5-7*). To date, induction of Abs that neutralize HIV-1 heterologous, difficult-to-neutralize HIV strains has not been achieved by vaccination. Here, we show vaccine induction in humans of HIV-1 antibodies capable of neutralizing multiple difficult-to-neutralize HIV-1 strains. The immunogen used was a HIV-1 envelope peptide complexed with a liposome that targets a membrane proximal external region (MPER) bnAb gp41-epitope (*8-10*). Successful MPER-directed bnAbs bind to both gp41 polypeptide and to

the adjacent virion lipid bilayer. Structural studies demonstrated multiple vaccine-induced modes of bnAb epitope recognition. BnAb B cell lineage analysis demonstrated that vaccine-induced antibodies had progressed to an intermediate stage of bnAb development, with incomplete ability to optimally bind to virion lipids, thus limiting full development of bnAb potency and breadth. Thus, this study demonstrates a proof-of-concept for vaccine induction of heterologous HIV-1 neutralizing B cell responses in humans and provides hope that development of a preventive antibody-inducing HIV-1 vaccine may ultimately be possible.

Introduction

Development of a preventive HIV-1 vaccine is a global priority. However, of ten HIV-1 vaccine efficacy trials, all showed no protective effect except the RV144 trial in Thailand that showed 31.2% estimated protection that was insufficient to deploy the vaccine (*11-13*). Moreover, a vaccine similar to that used in RV144 was tested against clade C HIV-1 in South Africa and showed no efficacy (*14*). HIV-1 envelope (Env)-containing vaccines tested to date have only induced non-neutralizing antibodies (nnAbs) that are postulated to mediate anti-viral activity by Fc receptor-mediated mechanisms (*11, 15*). However, no previous vaccine efficacy trials induced broadly neutralizing antibodies (bnAbs) (*1, 2, 13, 16*). With the failure of nnAb vaccines, attention has turned to developing an HIV-1 vaccine that can induce bnAbs (*1, 2*).

Most bnAbs identified to date from HIV-1-infected humans have unusual traits, such as long third heavy chain complementary determinant regions (HCDR3s), high levels of improbable mutations (*17-19*), and/or polyreactivity with host or environmental antigens (*4, 20, 21*). The unusual traits required for bnAb activity may be disfavored by tolerance mechanisms of the immune system, such as deletion or anergy (*22-25*). The HIV-1 Env is heavily glycosylated with host, high mannose and complex glycans that are poorly immunogenic and shield a major portion of the Env surface (*26*).

One Env target for bnAb induction is the membrane proximal external region (MPER) on gp41 Env (*27*). Distal-MPER targeted Abs are among the most broad bnAbs that have been isolated (*28-31*), while prototype bnAbs targeting the proximal MPER have more limited neutralization breadth (*32*). MPER bnAb epitopes are physically located near the virion lipid membrane, and for most MPER bnAbs, the lipid membrane is a component of the bnAb epitope (*20, 33-35*). Binding to lipids has been proposed to tether the bnAb on the virion membrane to enable binding to gp41 neutralizing MPER bnAb epitopes upon their exposure by Env receptor-mediated activation (*34*). However, induction of Abs to self-lipids has been difficult and proposed to be a roadblock in MPER bnAb induction (*20, 36*). Proximal MPER NAb precursors have paratopes that can recognize MPER epitopes, but lack the ability to bind lipids and tether to the virion membrane (*37*). A neutralization assay that detects MPER precursors has been developed that promotes tethering of MPER-reactive Abs to cell surface via FcγRI/CD64 expression in the TZM-bl infection indicator cell line (*37-39*).

BnAbs have been shown to protect monkeys from simian human immunodeficiency virus (SHIV) challenges (*40-42*), and to be effective against susceptible HIV-1 strains in prevention of transmission in humans (*43*). Potent bnAbs develop in HIV-1-infected humans, but only rarely, and after many months to years after transmission (*7, 18, 19, 44*). A strategy for inducing bnAbs, termed B cell lineage immunogen design, selects or constructs Envs that can bind with high affinity to bnAb lineage naïve or unmutated common ancestor (UCA) B cell lineage precursors, and then guide bnAb development from early intermediate to mature bnAbs by sequential immunizations (*13, 21*). A number of studies have demonstrated that immunogens that bind to CD4 binding site UCA B cell receptors can expand bnAb precursors in animal models (*41, 45-47*) and now in humans (*48*). A second strategy is epitope-focused immunogen design whereby a linear peptide or structural epitope is targeted by repeated immunizations (*9, 37, 49, 50*). We have designed a MPER peptide-liposome with proximal and distal MPER bnAb

epitopes plus lipids (*8-10*) and demonstrated induction of Abs in rhesus macaques that neutralize HIV-1 in the TZM-bl/FcγRI neutralization assay, but did not neutralize HIV-1 in the TZM-bl assay (*37*). However, to date, there has been no success of any Env immunogens in humans in inducing bnAb precursors to mature to the stage of neutralizing heterologous tier 2 difficult-to-neutralize HIV-1 in the TZM-bl assay.

The HVTN133 (NCT03934541) trial tested the MPER peptide-liposome in 20 HIV-1 naïve individuals (*51*). Here, we demonstrate induction of polyclonal MPER epitope-targeted Abs that neutralized heterologous HIV-1 strains. Moreover, the most potent vaccine-induced MPER clonal B cell lineage underwent sufficient affinity maturation after three immunizations to acquire neutralization of 35% of heterologous clade B tier 2 (difficult-to-neutralize) HIV-1 strains. These data demonstrate the induction of heterologous tier 2 virus nAbs in the TZM-bl neutralization assay in humans.

Results

Frequency of MPER-reactive B cells

The immunogen used in the HVTN133 trial was a MPER peptide-liposome designed to mimic the interactions of prototype MPER bnAbs 2F5 and 4E10 with epitopes in HIV-1 gp41 (*8-10*). The HVTN133 trial was halted due to an anaphylaxis reaction thought to be due to polyethylene glycol (PEG) in the immunogen (*51*) after 20 participants had received 2 immunizations and 5 participants had received 3 of 4 planned immunizations (**Figures 1a-1b**).

First, we performed MPER+ antigen-specific B cell sorting on CD19+ B cells from peripheral blood cells (PBMCs) at pre-vaccination and after the 3rd immunization to interrogate the most mature vaccine-induced B cell responses (**Figure 1c**). We isolated 510 B cells from 5 HVTN133 vaccine trial participants after the 3rd immunization using fluorophore-labeled MPER-peptide hooks, and after expression of memory B cell receptors (BCRs) as recombinant IgG1

Abs, we identified 87 binding MPER+ Abs with OD@450nm ≥0.5 in ELISA (**Table S1**). Vaccinees 133-23 and 133-39 had the highest number of post-3rd immunization circulating B cells specific for the MPER ligand (**Tables S1-S2**). MPER+ recombinant Abs were those that bound to the vaccine-matched MPER656 peptide (^{656}NEQELLELDKWASLWNWFNITNWLW^{680}) or the MPER.03 (KKK^{656}NEQELLELDKWASLWNWFDITNWLWYI^{682}RKKK) peptide. MPER-differential (Δ) binding Abs were those that bound to a wild-type (WT) MPER.03 peptide and ≥2.5X less to a mutant MPER.03 peptide with knockout (KO) mutations of MPER bnAb epitopes (D664A, W672A) (*37*) (**Table S3**). MPERΔ Abs constituted 86% (75/87) of total MPER+ Abs (**Tables S1-S3**). Immunization with the MPER peptide-liposome boosted the frequency of MPER precursors from ≤ 1/1,000,000 to ~1/11,100 in vaccinee 133-23 and to ~1/25,000 B cells in vaccinee 133-39 (**Tables S1-S2**).

Vaccine-induced MPER+ Abs

The variable heavy (V_H) genes used in MPER+ antibodies isolated from post-3rd immunization MPER+ B cells were polyclonal and predominantly V_H7-4-1 (31/87, 36%) that is novel in a bnAb; V_H5-51 (30/87, 34%) used by prototype MPER bnAbs, m66 and m66.6 (*32*); V_H2-5 (10/87, 11%) used by prototype MPER bnAb, 2F5 (*52*); and V_H3-49 (9/87 (10%), also novel as an MPER nAb (**Figures 1d-1e; Table S4**). These frequencies were higher than in 209,523 paired IgH sequences of antigen-unbiased Abs in pre-vaccination blood samples from the same five HVTN 133 participants (**Figure 1d; Table S5**). The light chains of post-vaccination MPER+ Abs were also polyclonal with the most common being Vκ4-1 (24/87, 28%), Vκ1-39 (17/87, 19%) and Vκ3-20 (16/87, 18%) (**Figure 1d; Table S4**). Additionally, while vaccine-induced MPER+ BCRs made as recombinant Abs had higher median heavy and light chain gene mutation frequencies compared with antigen-unbiased Abs in the same vaccinees prior to vaccination (**Figures 1f, S1A**), they were not as mutated as prototype MPER bnAbs (8). MPER+ Abs using V_H2-5 and V_H3-49 genes had the shortest HCDR3 lengths of 11 and 9 amino

acids (aa), respectively, while those using V_H7-4-1 and V_H5-51 genes had longer HCDR3 lengths ranging up to 23-26 amino acids (**Figures 1g, S1b**).

Polyreactivity is a common trait of MPER bnAbs (*20, 33, 53*). MPER bnAb 2F5 cross-reacts with human protein kynureninase (KYNU) that contains an MPER-bnAb epitope shared with the gp41 sequence of ^{662}ELDKWA^{667} (*53, 54*). Overall, 29/87 (33%) vaccine-induced recombinant MPER+ Abs demonstrated binding to KYNU, clinical autoantigens and/or cardiolipin (**Table S6**). Thirteen of 16 KYNU-reactive Abs demonstrated ≥3 fold reduction in binding to a KYNU-KO (D664E) (*54*) protein (referred to as KYNU-Δ binders), and 10/13 KYNU-Δ Abs used V_H2-5 also used by 2F5 (**Table S6**). V_H2-5 MPER+ Abs were most polyreactive; 10/10 KYNU-Δ, 5/10 cardiolipin+, and 7/10 were positive for reactivity with host autoantigens (**Figure 1e, Table S6**). However, the V_H2-5 putative 2F5-like Abs had HCDR3s of only 11 aa (**Figure 1g**) and thus were unlikely to progress to bnAbs similar to 2F5 with HCDR3s of 24 aa.

The 2F5 bnAb unmutated ancestor (UA) and mature 2F5 bnAb target the proximal-MPER epitope that includes DKW in SP62 peptide (^{652}QQEKNEQELLELDKWASLWN^{671}) (*9*). We found that the majority of MPER+ Abs (67/87, 77%) of the vaccine-induced MPER+ Abs bound SP62 peptide encoding proximal MPER bnAb epitope with heterogeneous patterns of epitope reactivity within ^{666}ELDKW^{670} (**Table S7**). There were no vaccine-induced Abs isolated that bound to the distal MPER bnAb epitope, ^{671}NWFNIT^{676}, although this aa sequence was present in the MPER peptide-liposome.

Neutralization Profiles of MPER+ Abs

MPER bnAbs bind gp41, and also bind to virion lipids to tether until the full MPER gp41-epitope is exposed following Env-CD4 binding (*33-35, 37*). The TZM-bl/FcγRI neutralization assay identifies MPER bnAb-precursors that bind to the MPER proximal or distal gp41-epitopes, but have not yet acquired mutations required for virion lipid binding (**Figure 2a**) (*37-39*). We

hypothesized that the TZM-bl/FcγRI neutralization assay would be more sensitive for detecting neutralization of tier 1 and 2 HIV-1 strains by HVTN 133 MPER+ Abs than the standard TZM-bl neutralization assay (*37*). Proximal MPER bnAbs are most potent for clade B HIV-1 strains (*32*). Thus, we assayed MPER+ and MPERΔ recombinant Abs for their ability to neutralize both easy-to-neutralize tier 1 (W61D, HXB2) and difficult-to-neutralize tier 2 (JRFL, SC44 and the transmitted-founder virus, WITO) clade B HIV-1 strains in both the TZM-bl/FcγRI and TZM-bl neutralization assays.

From 87 vaccine-induced MPER+ Abs that constituted 38 unique clonal lineages, we selected 80 mAbs representative of the 38 clones and tested them for HIV-1 neutralization in TZM-bl and TZM-bl/FcγRI cells (**Figure 2b**). Forty-nine of 80 MPER+ Abs (61%) neutralized tier 1 and/or tier 2 HIV-1 strains in the TZM-bl/FcγR1 neutralization assay (**Table S8**). The 49 MPER+ nAbs constituted 24 clonal lineages and used six different heavy chain genes (V_H7-4-1, V_H5-51, V_H3-49, V_H2-5, V_H1-69, and V_H3-73) (**Figures 2c, S4; Table S8**), with HCDR3 lengths ranging from 9-26 amino acids (**Figure S1c**), thus demonstrating a polyclonal nAb response. The geometric mean IC50 neutralization titers for the 24 neutralizing B cell clones for the tier 1 and tier 2 above viruses in the TZM-bl/FcγRI neutralization assay ranged from 0.18 µg/ml to 0.05 µg/ml (**Figure 2c**). Of the 24 B cell clonal lineages that neutralized in the TZM-bl/FcγRI neutralization assay, 14 also neutralized heterologous tier 1 HIV-1 in the standard TZM-bl assay with geometric mean IC50 neutralization titers for W61D (4.2 µg/ml) and HXB2 (10 µg/ml) (**Table S8**). Within the 24 B cell clonal lineages that neutralized tier 1 HIV-1 strains in the TZM-bl assay, we also found two clonal lineages, the single DH1425 nAb and an 11-member clonal lineage, DH1317, that neutralized heterologous HIV-1 tier 2 strains in the TZM-bl assay (**Figure 2c, Tables S8 and S10**).

Heterologous Tier 2 Neutralization in the TZM-bl Assay

V_H7-4-1 is a rare heavy chain gene in the B cell repertoire expressed at less than 1% (**Table S5**), although it was the most common V_H used in MPER+ BCRs (**Figure 1e, Table S4**). Both tier 2 virus-neutralizing clonal lineages used the V_H7-4-1 gene (**Figure 2c).** Of two alleles, V_H7-4-1*02 is most common, and occurs in ~60% of individuals (*55*). Poor expression of the V_H7-4-01*01 allele is due to an unpaired cysteine at heavy chain gene position 92 that compromises Ab expression (*55*). Of the 5 HVTN 133 vaccinees who received three immunizations, only two, 133-23 and 133-39 had the highest V_H7-4-1 transcript frequencies suggestive of the V_H7-4-1*02 allele, and these two vaccinees were the best NAb responders and gave rise to both of the V_H7-4-1 tier 2 virus neutralizing clonal lineages (**Figure S1d**).

V_H7-4-1 neutralizing B cell clonal lineage contains 11 IgG MPER+ Abs with a 15 aa HCDR3 and nucleotide mutation frequencies of ~2-6%, paired with Vκ1-12 gene (**Figure S2a, Table S9**). Analysis of the DH1317 clonal lineage members using the SP62 MPER alanine scanning peptide set demonstrated predominant dependence on the D^{664} of the ^{662}ELDKWA^{667} epitope (**Figure 3a and Table S7**). However, binding contacts with additional residues were likely since several members of the lineage (DH1317.4, DH13417.8, DH1317.9) showed ~5-fold reduced binding to the mutant K665A peptide, as well as to E657A, L660A, or E662A (**Table S10**). In addition, six DH1317 clonal lineage members were polyreactive for host antigens (**Table S6**).

DH1317 Abs neutralized both tier 1 and tier 2 viruses in the TZM-bl assay, with neutralization enhanced 2 logs in the TZM-bl/FcγRI assay (**Figure 2c and Table S11**). We found that 8/11 DH1317 B cell lineage member Abs and 4 inferred intermediate Abs (IA) neutralized both tier 1 and 2 heterologous HIV-1 strains in the TZM-bl assay, while 3/8 DH1317 mature Abs neutralized only tier 1 in the TZM-bl assay (**Table S11**). All DH1317 mature nAbs as well as computationally inferred unmutated common ancestor (UCA) and IA (*56-58*) nAbs demonstrated enhanced neutralization potency and breadth in TZM-bl/FcγRI cells (**Table S11**). The DH1317 UCA and IA Abs neutralized tier 1 and 2 HIV strains in TZM-bl/FcγRI cells, while the UCA and

initial intermediate I10 only neutralized tier 1 HIV strain in TZM-bl/FcγRI cells (**Table S11**). Thus, the sequence of vaccine-induced affinity maturation of proximal MPER nAb activity is, a) sequential acquisition of the ability to neutralize tier 1 and tier 2 HIV-1 in the TZM-bl/FcγRI assay, b) neutralization of tier 1 HIV-1 in the TZM-bl assay, and finally c) acquisition of neutralization in the TZM-bl assay of tier 2 HIV-1 strains (**Figure 2a**).

DH1317.4 and DH1317.9 Abs demonstrated the most potent neutralization of tier 2 clade B HIV-1 strains in TZM-bl cells (**Figure 2c and Table S11**). DH1317.4 neutralized 29/197 (15%) multiclade HIV-1 strains in the TZM-bl assay, including 35% of clade B HIV-1 strains (**Figure S3**). Of 125 non-clade B HIV-1 strains, DH1317.4 neutralized only two clade G viruses and one recombinant clade CD virus (**Figure S3**).

A major roadblock to bnAb development is the need for improbable bnAb lineage mutations (*17*). **Figure S4** shows the clonal tree of the DH1317 B cell lineage with improbable mutations (<2% frequency of occurrence) needed for heterologous neutralization acquisition. Thus, the MPER-peptide liposome selected for a number of improbable mutations resulting in tier 2 heterologous neutralizing activity in most members of the DH1317 B cell lineage.

To determine if lack of neutralization of non-clade B strains was due to lack of binding to the antibody Fab paratope or to insufficient lipid binding, we tested neutralizing nAbs DH1317.4 and DH1317.9 for their ability to neutralize non-clade B viruses in the TZM-bl/FcγRI assay. Both DH1317.4 and DH1317.9 neutralized 7/19 HIV-1 strains in the TZM-bl/FcγRI assay selected for their neutralization resistance to DH1317.4 or DH1317.9 Abs in the TZM-bl assay. Those tier 2 HIV-1 strains neutralized in the TZM-bl/FcγRI assay included clades A (1/2), C (1/3), recombinant AG (2/3) and B (3/5) pseudoviruses, the latter from placebo recipients who acquired HIV-1 infection in the recent Antibody Mediated Protection (AMP) trials (NCT02716675, NCT02568215)] (**Figure 3b**). These data demonstrated that the paratope of

DH1317 nAbs was in a conformation capable of binding to the neutralizing gp41 epitope in the 7 neutralized HIV-1 strains, but required FcγRI tethering on TZM-bl cells for neutralization activity, indicating insufficient Ab virion lipid reactivity for TZM-bl assay neutralization.

One additional single V_H7-4-1-using Ab, DH1425, was also found that reproducibly neutralized the tier 2 HIV-1 JRFL strain in the TZM-bl assay with IC50 of 37 µg/ml (**Figure 2c**). DH1425 is a 14 aa long HCDR3 nAb paired with Vκ3-20 (**Table S9**). Thus, these data in DH1317, DH1425 and other heterologous neutralizing B cell lineages indicated that while bnAb maturation in vaccinated humans in the HVTN 133 trial had proceeded further towards bnAb breadth and potency than in any previous study in humans, nAb B cell maturation after 3 immunizations was incomplete for optimal bnAb B cell development.

A neutralization signature analysis of the 197 HIV-1 strains with DH1317.4 compared to the prototype proximal MPER bnAb, 2F5, demonstrated that DH1317.4 had similar resistance signatures as 2F5, but that 2F5 tolerated more resistance signatures as a bnAb with more breadth compared to DH1317.4. While 2F5 had better recognition of ^{658}K, ^{659}D, ^{662}A, ^{667}N and ^{668}N than DH1317.4, it could not recognize ^{665}S or ^{667}K (**Figure S5**). When compared to prototype bnAbs m66.6 as well as 2F5, DH1317.4 had similar neutralization profiles both in terms of correlation of neutralization potency as well as with overlap of commonly sensitive or resistant viruses (**Figure S6)**. Thus, neutralization resistance to non-clade B strains can in part be explained by inability to recognize MPER bnAb epitope amino acid variability.

Serum NAb Assay

In a companion paper reporting the clinical and serum serologic analysis of the HVTN133 trial, there was no detectable HIV-1 neutralization activity in HVTN 133 participants' serum in the TZM-bl assay (*51*). In contrast, in HVTN133 vaccinees, we isolated blood B cells with BCRS that when expressed as recombinant Abs, neutralized tier 2 heterologous HIV-1. To

address the conundrum of why tier 2 HIV-1 nAbs could not be detected in post-vaccination serum, we asked if tier 2 virus neutralizing antibodies could be identified in serum from the two best responders (133-123 and 133-39). We compared purified total serum IgG with affinity purified MPER+ IgG (see methods) for the ability to neutralize the tier 1 HIV strain W61D and the tier 2 HIV strains, JRFL and WITO. Purified total IgG had low or no observable neutralizing activity (**Figure S7**). In contrast, concentrated MPER+ affinity-purified IgG did have significant neutralizing activity in the TZM-bl assay for tier 2 viruses JRFL and WITO when compared to total IgG ($p = 0.024$ for JRFL and 0.0477 for WITO, Exact Wilcoxon Test) (**Figure S7**), demonstrating that the lack of tier 2 virus neutralizing activity in serum is due to low levels of serum nAbs that are below the limit of detection (1:10 serum dilution) in the TZM-bl neutralization assay.

Structural Analyses of DH1317 NAbs

We first performed negative-stained electron microscopy (NSEM) on 7 neutralizing B cell clonal lineages [DH1317, DH1319, DH1322 and DH1346 (V_H7-4-1); DH1321 (V_H5-51); DH1318 (V_H3-49); and DH1316 (V_H2-5)] and 2 prototype bnAbs (M66.6 and 2F5) that mapped to residues in the MPER bnAb epitope ^{662}ELDKWA^{667} (**Figures 3c, S8 and S9**). To obtain lower resolution structures in complex with a trimer-MPER protein, we expressed a detergent micelle-bound trimer encoding MPER (JRFL SOSIP.683) (**Figure S8)** (*59*), produced Fabs and visualized the Fab-trimer complexes by NSEM (**Figure 3c)**. Both the prototypic bnAbs and HVTN133 Abs bound to the MPER epitope in the JRFL trimer in a similar manner. Although the MPER was flexible in this Env construct, the DH1321.1 V_H5-51 nAb appeared similar to bnAb M66.6 while the DH1318 V_H3-49 nAb was the most similar in orientation to prototype bnAb 2F5. Both M66.6 and 2F5 prototype bnAbs have long HCDR3s (*32*). Interestingly, V_H2-5 nAb DH1316.8, V_H3-49 nAb DH1318.2 have short HCDR3s of 11 and 9 aa, respectively, yet neutralize HIV-1, and the best bnAb DH1317.4 has an HCDR3 of 15 aa. Whether MPER Abs

with shorter HCDR3s of 11 or 9 aa can affinity mature to greater breadth and potency or whether will be limited in bnAb activity is not known.

To assess the structural basis for DH1317, DH1322 and DH1346 V_H7-4-1 nAb recognition of gp41 MPER, we co-crystallized their fragments of antigen binding (Fabs) in complex with MPER peptides (**Figures 4 and S10; Table S12**). Fab structures of variants DH1317.8 and DH1322.1 were determined to 2.4 and 2.0 Å resolution, respectively, in complex with MPER proximal peptides spanning gp41 residues 652-671 and 651-671, respectively. The structure of clone DH1346 was determined to 2.0 Å resolution in complex with an extended MPER peptide spanning gp41 residues 656-683 (**Figures 4 and 5, S10 and S11; Tables S12 and S13**).

All three V_H7-4-1 Abs recognized a similar helical conformation of the gp41 MPER proximal epitope (**Figures 4a, 5a and S10**). Ordered regions of the bound peptides commenced with residues N656 or E657 and extended to residues W670, N671, and K683 for DH1317.8, DH1322.1, and DH1346, respectively. In total, buried interfaces on MPER ranged from 709-865 $Å^2$, while those on the Abs ranged from 615-798 $Å^2$, with the heavy and light chains accounted for 70-80% and 20-30% of the interfaces, respectively **(Figures 4f, 5d, 5e and Table S13)**. Superposition of the three complexes by aligning their common V_H7-4-1 regions revealed that the three nAbs approached MPER from similar angles and recognized the same face of the MPER proximal helix, one that included residue D664 (**Figure 4d**). Closer examination of D664 interactions revealed that it nestled into a pocket formed between the Ab heavy and light chains in all three nAbs **(Figure S11a)**. D664 interactions within this pocket were anchored by a salt bridge in all three complexes, although in each case mediated by distinct Ab arginine residues: HCDR3 R97 in DH1317.8, LCDR3 R95a in DH1322.1, and LCDR3 R91 in DH1346 **(Figures 4e, 4g and S11a)**.

Since the disparate light chains and HCDR3 loops of DH1317.8, DH1322.1 and DH1346 did not alter their common modes of MPER recognition, we next assessed the contribution of

their shared V_H7-4-1 genes to epitope recognition, and found a nearly identical set of residues across the three Abs (**Figure 4f**). These interfacial residues fell predominantly within V_H7-4-1-encoded HCDR1 and HCDR2 loops, and exhibited similar patterns of residue buried surface areas (**Figure 4f**). While ~4 out of 9 of these V_H7-4-1 residue positions exhibited somatic mutations, contacts between them and gp41 were nonetheless conserved (**Figures 4f-4g**). Specifically, HCDR1 residues contacted gp41 residues E657 and Q658 in all three complexes, while HCDR2 residues commonly contacted gp41 residues Q658, L661, E662, and K665 in all three nAbs (**Figure 4g**). Thus, the x-ray crystallographic structural analysis of a polyclonal set of V_H7-4-1-using nAbs revealed a novel shared mode of proximal MPER recognition that is permissive for use of diverse light chains and heavy chain-encoded CDR3 loops.

We next compared the modes of proximal MPER recognition of the V_H7-4-1-using nAbs against those of previously characterized Abs that target this region; an MPER bnAb-precursor Ab, DH570, derived from a rhesus macaque immunized with the MPER peptide-liposome that neutralized HIV-1 in the TZM-bl/FcγRI assay (PDB 5DD0) (*37*), and the prototype proximal MPER bnAbs m66 (PDB 4NRX) and 2F5 (PDB 1TJI) (**Figure 5**) (*32, 60, 61*). DH570-bound MPER adopted an exclusively helical conformation, similar to that of V_H7-4-1-using NAbs, while m66-bound MPER adopted a structurally hybrid conformation that is helical between residues 658-664 but a coil otherwise (**Figure 5a**) (PDB 4NRX) (*60*). 2F5-bound MPER exclusively adopted an extended coil conformation (**Figure 5a**) (PDB 1TJI) (*61*). Superposition of the helical regions of DH570- and m66-bound epitopes to that of V_H7-4-1 nAb DH1322.1, which was used as a reference, revealed that DH570 approached from a similar direction as the V_H7-4-1 using nAbs, while m66 approached a face of the proximal MPER helix that was opposite to the V_H7-4-1 using nAbs **(Figure 5b-5c)**. Alignment of 2F5 structurally homologous regions to bound m66 peptide (namely residues 664-666) suggested that 2F5 approached the gp41 MPER from a direction similar to that of m66 (**Figure 5a-5c**). Buried surface areas (BSA) along MPER for the

three V_H7-4-1-using nAbs as well as for prototype MPER Abs DH570, m66, and 2F5 revealed the three V_H7-4-1-using nAbs mediated interactions with a nearly identical set of residues on gp41 and with similar degrees of buried surface per residue, while MPER interface residues of DH570, m66, and 2F5 exhibited a pattern of interaction distinct from that observed for the V_H7-4-1-using nAbs (**Figure 5a, 5e**). DH570 and m66 were similar to V_H7-4-1 Abs in that they recognized fully or partially helical conformations of proximal MPER, and in the case of rhesus macaque Ab, DH570, also approached from a similar direction. However, DH570 and m66, as well as 2F5, interacted with sets of residues on MPER that were distinct from those bound by V_H7-4-1-using nAbs (**Figure 5d-5e**).

Lipid Binding of DH1317 BnAbs

Previous studies have reported lipid reactivity as a feature of MPER+ bnAbs (*20, 30, 33, 35*), with a role for the CDRH3 hydrophobic loop in lipid binding and neutralization, as well as the involvement of CDRH1 loop in binding to lipid head groups (*35*). Examination of the pre-CDRH1 residues in DH1317 lineage, as well as other V_H7-4-1 nAb members, revealed that the putative lipid head group-binding CDRH1 sequences were similar (**Figure S12a**). However, the V_H7-4-1 Abs, including members of DH1317 lineage, did not bind equally to liposomes containing phosphatidylglycerol (PG) (**Figure 6a, S12b**), a lipid ligand for the MPER bnAb, 4E10 (*35*). It is notable that Abs with weaker PG-lipid binding had negatively charged residues adjacent to the conserved pre-CDRH1 residues (**Figure S12a**) that potentially could impede lipid binding due to charge hindrance. For the heterologous nAb clonal lineage, DH1317, a significant correlation was observed between PG-lipid binding and HIV-1 W61D neutralization potency (Kendall's Tau correlation coefficient =0.6363, P=0.0054) (**Figure 6b**).

We next computed lipid insertion propensity scores (ΔG_{wif}) (*37*) of amino acids in the CDRs of each mature DH1317 lineage neutralizing Ab, as well as inferred Ab intermediates and UCA in the DH1317 lineage (**Table S14**). The ΔG_{wif} scores corresponding to more favorable lipid

insertion propensity were also associated with higher HIV-1 W61D pseudovirus neutralization potency (**Figure 6c**). We also observed more favorable ΔG_{wif} lipid insertion scores in the overall set of W61D neutralizing Abs (n=27) compared to non-neutralizing Abs (n=56) (**Figure 6d, Table S15**). Regarding ΔG_{wif} total CDR scores, HVTN133 induced Abs were more similar to the prototype MPER bnab, m66.6 than to MPER bnAb 2F5.

Each of the DH1317 nAbs bound to MPER peptide-liposomes, and were able to recognize MPER epitopes in the context of the lipid membrane (**Figure S13**). However, the mode of binding to MPER peptide-liposomes were different when DH1317.4 that neutralized tier 2 viruses was compared to the DH1317.8 Ab that neutralized only tier 1 viruses in the TZM-bl assay. Binding of DH1317.4 to MPER liposomes could be fit to a sequential 2-step conformational change model, a binding profile previously described for MPER bnAbs that interact sequentially with lipids and MPER epitopes (*30, 33, 34, 37*), whereas the DH1317.8 could not (**Figure 6e**). Thus, the heterologous tier 2 nAb, DH1317.4, displayed similar binding properties to prototype proximal and distal MPER bnAbs (2F5, 4E10, DH511 and 10E8) with regard to interactions with phospholipid and mode of interactions with MPER peptide-liposome (*10, 30*).

Discussion

Here we have demonstrated that a vaccine containing HIV-1 gp41 MPER peptide-liposomes induced in humans a polyclonal MPER-directed B cell repertoire response made up of ~60% heterologous neutralizing antibody B cell clones and 40% non-neutralizing B cell clones. Each of the neutralizing B cell clones neutralized heterologous tier 1 or tier 2 HIV-1 strains in TZM-bl/FcγRI cells and 53% of these neutralizing clonal lineages also neutralized heterologous HIV-1 strains in the standard TZM-bl assay. Of the clones that neutralized in the TZM-bl assay, two progressed to neutralize tier 2 HIV-1 strains. While induced heterologous neutralizing activity

was primarily targeted to clade B with only 4/123 non-clade B viruses neutralized in the TZM-bl assay (**Figure S3**), we found clade A, C, and recombinant AG strains that, while not neutralized in the TZM-bl assay, were neutralized in TZM-bl/FcγRI cells, indicating that the nAb paratope bound well but did not have sufficient lipid tethering to neutralize non-clade B strains (**Figure 3b**). Thus, the induced MPER bnAb lineages were at early to late intermediate stages of MPER HIV-1 bnAb development (**Figure 2a**).

There are important implications of this study. We and others have previously demonstrated in MPER unmutated ancestor or mature MPER bnAb KI mice that full maturation of MPER bnAbs is limited by immune tolerance, both in the bone marrow and in peripheral B cell development stages (*25, 36, 37, 53*). While the distal MPER bnAb 4E10 maturation in 4E10 knock-in mouse is limited by tolerance to lipids, the proximal MPER bnAb in 2F5 is limited by tolerance to the tryptophan enzyme, kynureninase ^{662}ELDKWA^{667} sequence (*37, 53, 54*). That MPER Abs that bind to lipids were induced in HVTN 133 suggests that vaccine-induced lipid-reactive Abs are not controlled by tolerance to lipids at least to the stage of maturation of nAb development reported here. Of note, this study was only able to complete 2-3 immunizations of 4 planned. Thus, one hypothesis is that reformulation of the MPER peptide-liposome without PEG and with additional boosting may increase antibody affinity maturation to acquire additional heterologous neutralization breadth and potency.

The MPER peptide-liposome was designed to target the 2F5 unmutated ancestor to induce 2F5-like MPER bnAbs (*9*). While 11% of MPER+ Abs selected by the MPER peptide-liposome use the V_H2-5 gene also used by bnAb 2F5, none had HCDR3s longer than 11 aa, directly demonstrating that vaccine induced V_H2-5, 2F5-like Abs with long HCDR3s are disfavored.

V_H7-4-1 Abs were positively selected by the MPER peptide-liposome. That tier 2 virus-neutralizing V_H7-4-1 B cell clonal lineages had some degree of lipid membrane binding and the degree of lipid binding correlated with neutralization potency, raises the hypothesis that lipids

may be required to be in subsequent boosting immunogens. Although only ~60% of individuals will be able to make V_H7-4-1 utilizing MPER bnAb lineages (*55*), it is encouraging that the MPER peptide-liposome induced a polyclonal response utilizing multiple heavy chain genes.

The field of HIV-1 vaccine development is working with several UCA-targeting immunogens to induce putative precursors of bnAbs (*45, 48, 62, 63*) in order to use sequential boosting immunogens (*21*) to select for improbable mutations (*17*) and induce full bnAb maturation. However, since only putative precursors have been induced thus far in these cases, it will not be certain such precursors have the capability to fully mature to potent and broad heterologous neutralization capacity until this has been accomplished in humans. Here, we demonstrate that the putative MPER bnAb precursors in the DH1317 B cell clonal lineage that neutralized only in the TZM-bl/FcγRI assay, underwent affinity maturation to neutralize tier 2 heterologous HIV-1 in the TZM-bl assay, thus proving their bnAb precursor status (**Figure 2a**).

The TZM-bl/FcγRI assay was designed to identify bnAb precursors with the correct paratope but lack hydrophobic amino acids in the HCDR3 or HCDR1 regions needed for virion lipid binding for optimal neutralization (*37-39*). However, CD64+ (FcγR1+) dendritic cells and macrophages are among the first cells to be targeted in mucosal transmitted transmitted-founder HIV-1 infection (*39*). It has been postulated that MPER or other gp41 targeted nAbs that are capable of binding FcγRI on macrophages and dendritic cells may be protective from HIV-1 transmission *in vivo* (*39*). Thus, this study now provides vaccine-induced human Abs that potently neutralize HIV-1 strains in the TZM-bl/FcγRI assay that can be tested for their ability to protect against SHIV transmission in rhesus macaques.

In summary, HIV-1 envelope-reactive Abs with heterologous neutralizing breadth have been induced in humans by an MPER-targeted HIV-1 immunogen. While most of the induced nAbs did not have sufficient lipid reactivity to broadly neutralize tier 2 viruses, some Abs did neutralize

tier 2 heterologous HIV-1, thus proving such Abs can indeed be induced in humans. Moreover, these data suggest that a similar lipid-gp41 complex may be designed to induce more potent and broad lipid-reactive proximal and distal MPER Abs.

Acknowledgments. Supported by the HHS, NIH, NIAID, Division of AIDS, Center for HIV/AIDS Vaccine Immunology-Immunogen Discovery (CHAVI-ID) grant AI100645, by the HHS, NIH, NIAID, Division of AIDS Consortia for HIV/AIDS Vaccine Discovery (CHAVD) grant AI144371, by the HHS, NIH, NIAID, Center for HIV Structural Biology grant U54 AI170752, and by a Collaboration for AIDS Vaccine Development (CAVD) grant, OPP1094352/INV-007688, from the Bill & Melinda Gates Foundation. We thank the DHVI program and finance teams for grant management, including Kelly Cuttle, Jordan Cocchiaro, Daniel Tonkin and Whitney Edwards-Beck. We would like to thank Ken Cronin and Parth Patel for technical support with Fab preparation, SPR epitope mapping and affinity measurements; Aria Arus-Altuz, Xiaozhi Lu, and Dapeng Li for technical support with flow cytometry B cell isolation and PCR amplification of Abs from sorted B cells; Sommer Holmes for technical support on recombinant Ab expression; and Ryan Tuck for support with making figures and tables. BCR repertoire sequencing at baseline in the HVTN133 vaccine recipients was done by the DHVI Viral Sequencing Analysis Core facility; we would like to thank Bhavna Hora for study management in the core facility. Data were collected at Southeast Regional Collaborative Access Team (SER-CAT) 22-ID beamline at the Advanced Photon Source, Argonne National Laboratory. Use of the Advanced Photon Source was supported by the U.S. Department of Energy, Office of Science, Office of Basic Energy Sciences, under Contract No. W-31-109-Eng-38. Use of the Stanford Synchrotron Radiation Lightsource, SLAC National Accelerator Laboratory, was supported by the U.S. Department of Energy, Office of Science, Office of Basic Energy Sciences under Contract No. DE-AC02-76SF00515.

Author Contributions. BFH conceived study, designed immunogen, reviewed all data, and wrote the paper; SMA designed immunogen, performed experiments, and wrote the paper; WW oversaw isolation of Abs and BCR sequencing and repertoire analysis, and wrote the paper; GO oversaw crystallography structural analysis; PA oversaw cryo-EM structural analyses; NE, SRW, and LRB were PIs of HVTN 133; DM, MS, and AE performed neutralization assays; RJE and KM performed NSEM; DWC performed flow sorting; MM generated B cell baits for flow sorting; JH isolated Abs from sorted cells and managed the pipeline for this process; MM and JH generated recombinant Abs and oversaw Ab distributions; RP, MB and AF performed serum experiments and/or characterized Abs for binding and epitope mapping; KA performed immunogen antigenicity testing, preparation of phospholipid containing liposomes, and SPR/BLI measurements and analysis of Ab binding to lipids and to MPER liposomes; SS, XH, and JL produced Envs for cryoEM analysis; AN, BMJ, and AA performed x-ray crystallography; IM and TE generated BCR sequences via 10X genomics assays; MB, HK and KW performed computational analysis; KOS oversaw recombinant protein expression; KC, MJE and LC oversaw the clinical trial and lab analyses by the HVTN.

Methods

Vaccine participants

In the HVTN 133 clinical trial (NCT03934541) twenty-four participants, including 20 vaccine and 4 placebo recipients, were enrolled and scheduled to receive four immunizations of the MPER-656 peptide/liposome immunogen. Vaccinees received either a low (group T1, 500 mcg) or high (group T2, 2000 mcg) MPER peptide-liposome dose regimen (**Figures 1A-1B**). Before completion of the scheduled vaccinations, however, the study was halted due to safety concerns. 20 participants received 2 MPER peptide liposome doses, and 5 received 5 MPER peptide-liposome doses prior to trial being halted. Informed consent was obtained by all participants and the trial was approved by the Patient Review Safety Committee at NIAID.

Ethical oversight - All ethical oversight and monitoring for implementation/running of the trial itself was through HVTN and Sponsor (DAIDS) standard operating procedures. The protocol was reviewed and approved by the institutional review boards at all sites (Brigham and Women's Hospital, Fenway, Columbia University, New York Blood Center, University of Alabama Birmingham, and Fred Hutchinson Cancer Research Center) and written informed consent was obtained from each participant prior to enrollment. When the trial was halted, the event was reviewed by the Protocol Safety Review Team (PSRT)-- which includes the investigators (protocol Chairs), protocol leadership, and clinical safety specialists, as well as by the HVTN Data and Safety Monitoring Board (DSMB).

Sample/patient identifiers - The numbers provided in the publication are not sample or patient IDs. They are specifically HVTN-provided "PubID" ("Publication ID") numbers-generated by HVTN as an extra layer of coding, beyond the already coded PTID #s. They are intended for use in presentations and publications.

Flow Cytometry Sorting of MPER+ B Cells

B Cell Sorting. Sorts of MPER-specific memory B cells were conducted as previously described (*37, 64*). Briefly, cryopreserved PBMCs were thawed and counted. Cells were labeled with optimized concentrations of the following fluorochrome-mAb conjugates: PerCP-Cy5.5 anti-human IgM (clone G20-127, BD Biosciences), PE anti-human IgD (clone IA6-2, BD Biosciences), PE-CF594 anti-human CD10 (clone HI10A, BD Biosciences), PE-Cy5 anti-human CD3 (HIT3a, BD Biosciences), PE-Cy5 anti-human CD235a (clone GA-R2, BD Biosciences), PE-Cy7 anti-human CD27 (clone O323, ThermoFisher), Alexa Fluor 700 anti-human CD38 (clone HB7, BD Biosciences), APC-Cy7 anti-human CD19 (clone SJ25C1, BD Biosciences), BV570 anti-human CD16 (clone 3G8, Biolegend), and BV605 anti-human CD4 (clone M5E2, Biolegend). Cells were also labeled with fluorochrome-labeled antigen baits, prepared as 4:1 molar mixtures of biotinylated MPR.03 peptide and Streptavidin-VioBright 515 (Miltenyi Biotec)

or Streptavidin-Alexa Fluor 647 (ThermoFisher). Labeling with LIVE/DEAD Aqua (ThermoFisher) allowed identification and exclusion of dead cells. The gating strategy identify to memory B cells was: $Aqua^{-}CD14^{-}CD16^{-}CD3^{-}CD235a^{-}CD19^{+}IgD^{-}$. Memory B cells that bound both MPR.03-VB515 and MPR.03-AF647 baits were sorted as single cells into wells of a 96-well plate containing PCR lysis buffer. Cells were sorted on a FACSAria IIu (BD Biosciences) using FACSDiva software version 8. Data were analyzed using FlowJo version 10 (BD Biosciences).

Fluorophor-conjugated MPER-peptide production. In order to produce enough conjugated peptide to stain at least 10 aliquots of 5 million cells each with excess for quality testing, 200µL of 0.2mg/mL biotinylated MPER.03 peptide ($KKK^{656}NEQELLELDKWASLWNWFDITNWLWYIRK^{684}KK$) (MW = 4678 Da) was measured out and divided into two parts (1.07nmol or 100µL each) to be conjugated to either VB515 streptavidin fluorophore (MW = 61,040 Da, commercially obtained from Millitenyi Biotec Cat#: 130-108-993) or AF647 streptavidin fluorophore (MW = 59,485 Da, commercially obtained from ThermoFisher Cat#: S21374) at a 4:1 molar ratio. To achieve a 4:1-part molar ratio of peptide to fluorophore, 53.5pmol (16.3µL) per addition of VB515 was measured for a total of 265pmol (81.5µL) and 53.5pmol (12.7µL) per addition of AF647 for a total of 265pmol (63.6µL). In an amber Eppendorf tube, the biotinylated MPER.03 peptide was incubated for 15 minutes on a continuous mixing device at room temperature with one addition of fluorophore. After the incubation, subsequent additions of fluorophore were added with 15-minute continuous mixing in between until all 5 additions were added. The conjugated peptide mixture was then diluted using 1X PBS +0.02% NaN_3 to a concentration of 3000nM. Similarly, the biotinylated MPER.03_D664AW672A mutant peptide was conjugated to the BV421 streptavidin fluorophore (MW = 133,400 Da, commercially obtained from BioLegend, Cat#: 405225). The amount of BV421 used was 73.8µL split into 5 additions of 14.8µL. The three conjugated peptides were stored at 4°C. To confirm usability for flow studies, the peptides were tested for binding to

antibody-coated beads against mixes of 20% positive beads (2F5, 13H11) and 80% negative beads (CH65). The conjugated peptides were serially diluted, mixed with the bead mixtures, incubated for 30 minutes at 4°C, gently aspirated and washed a total of 3 times using 1X PBS +0.02%NaN_3 and ran in flow cytometry.

PCR isolation of Abs from antigen-specific B cell sorts

Single sorted B cells were obtained from HVTN133 vaccine recipients using previously described flow cytometry-based sorts (*37, 64*). Cells were individually sorted into 96 well plates containing lysis buffer and immediately stored at -80. Human V_HDJ_H and V_LJ_L segments were isolated by single-cell PCR (*64, 65*). Antibody sequences were analyzed using a custom-built bioinformatics pipeline for base-calling, contig assembly, quality trimming, immunogenetic annotation with Cloanalyst (https://www.bu.edu/computationalimmunology/research/software/), VDJ sequence quality filtering, functionality assessment, and isotyping as described (*56*).

Recombinant Ab production

Recombinant Abs were generated in large quantities by using commercially-obtained (GeneScript, Piscataway, NJ) plasmids with antibody heavy and light chain genes to transfect Expi 293i cells using ExpiFectamine 293 transfection reagents (Life Technologies, GIBCO; Cat#A14524) as described (*15*). The purified recombinant Abs were stored at 4°C in a citrate buffer (pH = 6.0). All recombinant Abs were expressed from plasmids containing a human or macaque IgG constant region and were QC'ed in Western Blot and Coomassie SDS PAGE for appropriate heavy and/or light chain protein expression.

VDJ sequencing of single B cells from peripheral blood

VDJ library construction and sequencing. Single Cell VDJ library construction was processed on 10X Chromium Controller (PN-1000204) using the Chromium Next GEM Single Cell 5' Kit v2, (PN-1000263) and BCR Amplification Kit (PN-1000253) following the manufacturer's protocols.

In brief, between 16,000 and 18,000 sorted B cells were loaded onto the Chromium controller to target the recovery ~10,000 cells for each sample. Final libraries were quantified using a TapeStation 2200 (Agilent) and Qubit 3 Fluorometer (Thermo Fisher). For BCR repertoire sequencing at baseline in HVTN133 vaccine recipients, we performed negative B cell enrichment from ~30M PBMCs in each experiment using a commercially available B cell enrichment kit according to manufacturer's protocol (StemCell Technologies; Vancouver, BC, Canada). The VDJ libraries were sequenced on the Illumina NovaSeq 6000 platform with Novaseq S4 Reagent kit (200 cycle kit) using the read parameters: 26 cycles for Read1, 10 cycles for i7 index, 10 cycles for i5 index, and 150 cycles for Read 2. We targeted 5,000 reads/cell for the VDJ libraries.

VDJ analysis: Illumina NGS generated BCR sequencing data was processed using the Cell Ranger single cell gene expression software provided by 10X Genomics. Reads were demultiplexed and quality filtered, followed by assembly and annotation using Cell Ranger 6.0.0 with the GRCh38 human V(D)J gene segment reference provided by 10X Genomics. Contigs assembled by Cell Ranger were re-annotated and analyzed using Cloanalyst (https://www.bu.edu/computationalimmunology/research/software/) with the default human Ig library to determine B cell immunogenetics and clonality as previously described (*56*).

Indirect binding ELISA

Ab binding was measured by ELISA in 384 well ELISA plates (Costar #3700) coated with 2mcg/ml streptavidin (Thermo Fisher Scientific Inc.. Cat. No. S-888) or protein antigen in 0.1M sodium bicarbonate overnight at 4C. Plates were washed with PBS/0.1% Tween-20 and blocked for one hour with assay diluent (PBS containing 4%(w/v) whey protein/15% Normal Goat Serum/0.5% Tween-20/ 0.05% Sodium Azide). Streptavidin coated plates were washed and followed by 10ul biotinylated peptide at 2mcg/ml in assay diluent for one hour. All plates were then washed and Abs added in 10µl volumes for 1 hour in three-fold serial dilutions

beginning at 100mcg/ml. Plates were washed and 10µl HRP conjugated goat anti-human secondary Ab (Jackson ImmunoResearch C:109-035-008) diluted to 1:15,000 in assay diluent without azide was incubated at for 1 hour, washed again and detected with 20µl SureBlue Reserve (Seracare 5120-0081) for 15 minutes. The Ab binding reactions were stopped with the addition of 20µl HCL stop solution and plates read at 450nm.

Polyreactivity binding assays

AtheNA: MAb reactivity to nine autoantigens was measured using the AtheNA Multi-Lyte ANA kit (Zeus scientific, Inc, #A21101). Abs were serially diluted for four 2-fold steps starting at 300µg/mL. The Abs were then diluted 1:6 in assay beads resulting in a final serial dilution of four 2-fold steps starting at 50 µg/mL in 50ul of beads. The kit SOP was followed for the remainder of the assay. Samples were analyzed using AtheNA software. An individual well was positive if >120 AU (Athena Units), negative if <100 and considered indeterminate if between 100-120. Any given Ab needed to be positive for two consecutive wells (i.e. to at least 25µg/ml) to be considered positive for autoreactivity; see values with yellow fill in **Table S6**.

Anti-cardiolipin reactivity. MAb reactivity to cardiolipin was measured using the Quanta Lite ACA IgG III kit (Inova Diagnostics, Inc.) by diluting Abs to final concentrations of 100, 50, 25 and 12.5µg/ml in sample diluent. 100ul of each sample was added to assay plates along with kit controls and the kit SOP was followed for the remainder of the assay. IgG phospholipid units (GPL) were calculated against a linear standard curve per kit instructions. An individual well was positive if GPL was >20, negative if <15 and indeterminate if between 15-20. Any given Ab needed to be positive for two consecutive wells (i.e. to at least 50µg/ml) to be considered cardiolipin positive; see values with yellow fill in **Table S6**.

Neutralization assays

NAbs were measured in either TZM-bl cells (*66*) or TZM-bl/FcγRI cells (*38*) as a function of reductions in luciferase (Luc) reporter gene expression as described (*67*). In both assays, a pre-titrated dose of virus was incubated with serial 3-fold or 5-fold dilutions of either serum (heat-inactivated 56^{o}C, 30 minutes), purified IgG or mAbs in duplicate in a total volume of 150 µl for 1 hr at 37^{o}C in 96-well flat-bottom culture plates. Freshly trypsinized cells (10,000 cells in 100 µl of growth medium containing 75 µg/ml DEAE dextran) were added to each well. One set of 8 control wells received cells + virus (virus control) and another set of 8 wells received cells only (background control). After 48 hours of incubation, 100 µl of cells was transferred to a 96-well black solid plate for measurements of luminescence using the Bright-Glo Luciferase Assay System (Promega). Neutralization titers are the dilution (serum samples) or concentration (purified IgG and mAbs) at which relative luminescence units (RLU) were reduced by 50% or 80% compared to virus control wells after subtraction of background RLUs. Assay stocks of molecularly cloned Env-pseudotyped viruses were prepared by transfection in 293T/17 cells (American Type Culture Collection) and titrated in TZM-bl cells as described (*67*).

Signature analyses and neutralization profile comparison

Env neutralization signature analyses for DH1317.4 and DH1317.9 were performed as previously described (*68*). Briefly, binary phenotypes of DH1317.4 and DH1317.9 sensitivity or resistance (IC50 >50 or <50µg/ml) were used. To correct for multiple testing, a false discovery rate (q-value) of <0.2 was used, and to correct for clade effects, phylogenetically corrected signatures were also calculated. Robust signature sites were identified by using the criteria that signatures at these sites had q < 0.2 and such sites were either in epitope sites (658 to 668) or had a phylogenetically corrected signature, or both. Signatures were visualized using sequence logos for the sensitive vs. resistant group of viruses (**Figure S5**) calculated using AnalyzeAlign tool on the Los Alamos HIV Databases (https://www.hiv.lanl.gov/content/sequence/ANALYZEALIGN/analyze_align.html). For

calculating inter-subtype variation at key signature sites in database strains, the “Filtered web” sequence alignment in AnalyzeAlign was used. For comparison of neutralization profiles between bNAbs, linear regression and Fisher’s exact test modules from SciPy were used (www.scipy.org) (*69*).

Ab binding to binary phospholipids

PC-PG binary lipids were prepared by mixing 1-palmitoyl-2-oleoyl-glycero-3-phosphocholine (POPC, Avanti) with 1,2-dioleoyl-sn-glycero-3-phospho-(1'-rac-glycerol) (18:1 (Δ9-Cis) PG, Avanti) that had been solubilized in chloroform to a concentration of 10mM with a 25:75 ratio of PC to PG. The PC-PG lipid mixture was dried under a steady stream of nitrogen and then placed in a vacuum for 3-4 hours to remove any trace amounts of chloroform. The lipids were rehydrated in 500uL of PBS 1X pH7.4 and incubated at 37°C for 45 minutes. After incubation, the lipid preparation was vortexed and sonicated for 45s followed by extrusion through a 0.1um polycarbonate membrane using a 1-mL mini-extruder (Avanti).

The binding of Abs was performed by surface plasmon resonance (SPR) using the Biacore3000 platform (Cytiva) in PBS 1X pH7.4 running buffer. A lipophilic L1 chip (Cytiva) was docked and prepared by immobilizing BSA 1% to a level of 2000-3000RU to reduce non-specific binding of mAbs. A 1:5 dilution of PC-PG in PBS 1X was prepared and then manually captured on the flow cells of the L1 chip at 5uL/min to a level of 400-500RU. At least one flow cell had no captured lipid and would be used for reference subtraction. After a series of wash steps, mAb diluted down to 100ug/mL was injected over the sensor surface at 20uL/min for 2 minutes followed by a dissociation of at least 5 minutes. 13H11 and 2F5 were used as negative and positive control mAbs, respectively. The lipid was then regenerated from the sensor using a 60s pulse of 40mM OGP at 100uL/min. Results were analyzed using BiaEvaluation Software (Cytiva). Binding to blank flow cells with no lipid capture was used for reference subtraction and to account for non-specific binding. Binding values were measured at the end of association

period and then normalized with respect to the variable lipid capture values. Reported results are an average of at least two measurements.

Lipid insertion propensity scores

Hydropathy analysis tool MPEx (*70*) (Membrane Protein Explorer) v3.3.0 with the water-interface scale was used to calculate lipid insertion propensity scores as the sum of ΔG_{wif}, the free energy of transfer of an amino acid from water to POPC interface (*71*), over all amino acids in the CDR regions of both light and heavy chains. CDR amino acid positions were defined using the software ANARCI (*72*) with the IMGT scheme. Custom R scripts were used to compute scores for all CDRs individually. Calculation and significance test for the Pearson correlation coefficients were performed using the R function stat_corr from package *ggpubr;* https://rpkgs.datanovia.com/ggpubr/).

Ab and Fab binding and titrations against MPER liposome immunogen

The binding of Abs to the MPER656 peptide-liposome immunogen (IDRI, Lot: 18P001) was performed using biolayer interferometry (BLI) and the OctetRed 96 system (Sartorius) in PBS 1X pH7.4 buffer. The sequence of MPER656-GTH1 peptide used in the MPER peptide-liposome is ^{656}NEQELLELDKWASLWNWFNITNWLWYIK^{683}YKRWIILGLNKIVRMYS). MPER peptide-liposomes were prepared at a 1:200 dilution in PBS and captured using APS (aminopropysilane) sensor tips to a level of approximately 1.0-1.5nm. The duration of liposome capture was 600s. The liposome loaded sensor tips were then coated with 0.01% BSA for 600s to block any non-specific interaction of the antibody with the sensor tips. The sensor tips were then washed with PBS for 120s. After washing with PBS 1x, the sensor tips were submerged into the mAbs (or Fabs) diluted down to 100µg/mL for an association length of 600. 13H11 was used as a negative control reference mAb while 2F5 and 2F5UA were used at positive control mAbs. Antibody binding analysis was performed using the ForteBio Data Analysis 10.0

software (Sartorius). The Y-axis was aligned to the baseline from 175s to 179.8s and the inter-step correction was aligned to dissociation. 13H11 binding was subtracted from the binding of each antibody for reference subtraction and to account for any non-specific binding. Binding curves are representative of one dataset.

For the Fab and mAb titrations against MPER656 peptide-liposomes, the same BLI procedure was performed as in the screening analysis. However, the samples were diluted from 1.25ug/mL to 50ug/mL and then individual MPER peptide-liposome captured sensors were submerged into these wells. Curve fitting analyses were performed in the BiaEvaluation Software (Cytiva) after 13H11 subtraction using the 1:1 model for most samples. For DH1317.4 Fab and DH1317.8 Fab, the two state conformational change model was used for fitting. Kinetic results and affinities are representative of one dataset.

F(ab) preparation from purified IgG samples.

F(ab) preparation was performed using a modified protocol previously described (1). Purified IgG samples were dialyzed into 20mM sodium phosphate, 10mM EDTA, pH 7.0 and then concentrated to 20mg/ml using centrifugal filtration (Amicon). IgGs were then digested using papain-agarose resin (Thermo Fisher Scientific) in 20mM sodium phosphate, 10mM EDTA, 20mM cysteine, pH7.4 for 5 hours at 37°C. A few select mAbs were digested with Lys-C instead of papain-agarose. F(ab) fragments were separated from undigested IgG and Fc fragments through a 1 hour incubation with rProtein A Sepharose Fast Flow (Cytiva). Finally, cysteine was removed by centrifugal filtration (Amicon) and buffer exchange to 1x PBS, pH 7.4.

Quality of F(ab) was measured via SDS-PAGE and size exclusion chromatography (SEC). SDS-PAGE was conducted by loading 2ug protein/lane on a 4% to 15% TGX stain-free gel (Bio-Rad) under reducing and nonreducing conditions. Loaded gels were run at 200V in Tris-glycine-SDS buffer. Bands were visualized using Gel Doc EZ imager (Bio-Rad), and band size was

assessed with a protein standard ladder (Bio-Rad). SEC was performed by loading 15ug protein on to a Superdex 200 increase 10/300 column using a 100-µl loop and run at 0.5ml/min using an Äkta Pure system (Cytiva). F(ab) peaks were analyzed with the system's Unicorn 7.6.0 software. Molecular weight was estimated using a linear regression calculated by running a mix of known-molecular-weight protein standards (Cytiva) on the same column.

Titrations of F(ab) to SP62 peptide and mutants

Affinities of F(ab)s to SP62 peptide (^{652}QQEKNEQELLELDKWASLWN^{671}) and alanine-substituted mutants were measured through Surface Plasmon Resonance (SPR) using a BIAcore S200 instrument (Cytiva) in HBS-EP+ 1x running buffer at 25°C. Biotinylated SP62 peptides and mutants were diluted to 20 ug/ml and injected over a streptavidin immobilized CM3 or CM4 chip surface at 5 uL/min. 80 – 120 response units (RU) of ligand was captured over flow cells 2 – 4. Flow cell 1 was used as a blank for reference subtraction of nonspecific binding to chip surface and streptavidin. Ligand capture was followed with long dissociation period of 30 mins or until response stabilized. F(ab)s were diluted to various concentration ranges between 0.25 nM and 400 nM and injected at a flow rate of 50 uL/min over flow cells 1 – 4 using single-cycle kinetics injection type. Six 120 s injections of F(ab) at increasing concentrations with 720 s dissociation after final injection. Chip surfaces were regenerated with Glycine, pH 2.0 for 30 s between cycles. Blank running buffer titration was used to account for signal drift in addition to the blank flow cell for double reference subtraction. Curve fitting of results was performed through BIAcore S200 evaluation software (Cytiva). Fitting made use of either heterogenous ligand model or 1:1 Langmuir model with global Rmax. Titration curves are representative of 2 data sets.

Protein expression and purification

Plasmid encoding JRFL.SOSIP.v6.683 was mixed with plasmid encoding furin in 1:4 ratio. This plasmid mixture was transfected in GnTI- cells (ATCC) at density of $2x10^6$ cells/ml using 293Fectin (Thermo Fisher) according to manufacturer's protocol. The cells were harvested 38-40 hours following transfection spinning down the transfected cell culture for 30 min at 3400 x g, and the supernatant was discarded. The cell pellet was solubilized with 200 ml lysis buffer (0.5% v/v Triton X-100, 50 mM Tris pH 7.4, 150 mM NaCl) with the addition of 2mg of PGT145 IgG and Pierce protease inhibitor tablets (Thermo Fisher) and incubated at 4°C for 30 min. The cell debris were spun down again at 4347 x g for 1 hour followed by filtration through a 0.8 µm filter. The supernatant was incubated overnight with 1 ml Ultra Protein A resin (Thermo Fisher) and 2 mg of VRC01 IgG at 4°C. On day 2 of the purification, the unbound cell lysate was removed by passing the resin containing supernatant over a gravity column. The resin was washed with 10 CV of each of the following buffers, buffer 1 (0.1% w/v CHAPS, 50 mM Tris pH 7.4, 150 mM NaCl, 0.03 mg/mL sodium deoxycholate), buffer 2 (0.1% w/v *n*-Dodecyl β-D-maltoside (DDM), 50 mM Tris pH 7.4, 500 mM NaCl, 0.03 mg/mL sodium deoxycholate), and buffer 3 (0.1% w/v DDM, 50 mM Tris pH 7.4, 150 mM NaCl, 0.03 mg/mL sodium deoxycholate, 2 mM EDTA) successively. The complex of Env with the IgG bound to the Protein A resin was digested on-column using Lys-C (1 µg Lys-C for 20 ug IgG) in wash buffer 3 at room temperature for 4 hours. Following digestion, the flow through containing the Fab-bound Env followed by a 5 CV wash of the resin with the SEC buffer (0.1% w/v DDM, 50 mM Tris pH 7.4, 150 mM NaCl, 0.03 mg/mL sodium deoxycholate), and concentrated using 100,000 MWCO concentrator to ~500 µL and further purified by size exclusion chromatography (SEC) using Superose 6 Increase 10/300 GL column (Cytiva) preequilibrated in SEC buffer.

Surface plasmon resonance measurement of Env trimer binding

Binding experiments for Fabs were performed using SPR on a Biacore T-200 (Cytiva, MA) with HBS buffer supplemented with 3 mM EDTA and 0.05% surfactant P-20 (HBS-EP+, Cytiva, MA).

All binding assays were performed at 25 °C. DH1317.4 Fab binding to JRFL.SOSIP.v6.683 was assessed using a Series S CM5 chip (Cytiva, MA) which was coated with anti-human IgG (fc) Ab using a Human Ab Capture Kit (Cytiva, MA). 2G12 IgG was captured on the anti-human Fc chip by flowing over a 200 nM solution for 120s at 5 µL/min flow rate, followed by Env at 200 nM (120s at 5 µL/min). DH1317.4 Fab was injected at concentrations ranging from 12.5 nM to 200 nM (prepared in a 2-fold serial dilution manner) over the chip surface using the single cycle kinetics mode with 5 concentrations per cycle. The surface was regenerated three pulses of a 3 M $MgCl_2$, pH 7.0 solution for 10 seconds at 100µL/min. Sensogram data were analyzed using the BiaEvaluation software (Cytiva, MA).

Protein Crystallization

Fragments of antigen binding (Fabs) of antibodies DH1317.8, DH1322.1, and DH1346 were buffer exchanged into 50 mM Sodium Acetate pH 5.2 and loaded onto a Mono S 5/50 ion exchange column (Cytiva) equilibrated in the same buffer. Loaded Fabs were eluted on a continuous gradient using 50 mM Sodium Acetate pH 5.2 supplemented with 500 mM Sodium Chloride, followed by size exclusion chromatography using a Superdex 200 Increase 10/300 column (Cytiva) equilibrated in gel filtration buffer (GFB) composed of 2.5 mM Tris Cl pH 7.5, 150 mM Sodium Chloride, and 0.002% sodium azide.

For purified DH1317.8 Fab, complexes were prepared with MPER peptides MPR.03, KKK^{656}NEQELLELDKWASLWNWFDITNWLWYIRK^{684}KK, and SP62, ^{652}QQEKNEQELLELDKWASLWN^{671}, at 3-fold molar excess. Sitting drop vapor diffusion crystallization screens were set up with a Mosquito Nanoliter Liquid Handling System (SPT Labtech, Concord, CA) using a total of 768 conditions (384 unique conditions for each complex) obtained from commercially available screens (Rigaku Reagents, Woodlands, TX, and Hampton Research, Aliso Viejo, CA). Diffracting crystals of the DH1317.8 Fab-SP62 peptide complex were obtained in condition composed of 20.1% Isopropanol, 10.05% PEG 8000, and 0.1M

Imidazole/Hydrochloric acid pH 6.5 which were optimized and cryoprotected in (2R,3R)-(−)-2,3-Butanediol prior to flash freezing in liquid nitrogen for data collection.

For purified DH1322.1 Fab, complexes were prepared with peptide K^{651}NQQEKNEQELLELDKWASLWN^{671}K at 3-fold molar excess. Sitting drop vapor diffusion crystallization screens were set up with a Mosquito Nanoliter Liquid Handling System (SPT Labtech, Concord, CA) using a total of 672 conditions obtained from commercially available screens (Rigaku Reagents, Woodlands, TX, and Hampton Research, Aliso Viejo, CA). Diffracting crystals were obtained in a condition composed of 25% PEG 1500 and 0.1M SPG buffer pH 8.5, which were flash frozen in liquid nitrogen for data collection.

For purified DH1346 Fab, complexes were prepared with peptide MPR.03 (see sequence above) at 3-fold molar excess. Sitting drop vapor diffusion crystallization screens were set up using Mosquito Nanoliter Liquid Handling System (SPT Labtech, Concord, CA) using a total of 672 conditions obtained from commercially available screens (Rigaku Reagents, Woodlands, TX, and Hampton Research, Aliso Viejo, CA). Diffracting crystals were obtained in a condition composed of 25% PEG 1500, 0.1M Sodium acetate/acetic acid pH4.5, 30% MPD, and 30% dextran sulfate sodium salt, which were flash frozen in liquid nitrogen for data collection.

Structure Determination and Analysis

X-ray diffraction data were collected at the ID-22 beamline (SERCAT) at the Advance Photon Source (Arognne, Il) or at the BM12-2 beamline at the Stanford Synchrotron Radiation Lightsource (Menlo Park, CA). Collected datasets were processed using HKL-2000 or XDS (*73, 74*). Structures were solved by molecular replacement using PHASER, with search model PDB 4NRX for DH1317.8, and the resulting DH1317.8 structure as a search model for DH132.1 and DH1346 (*75*). Refinement was carried out using PHENIX with manual iterative model building in Coot (*76, 77*). Protein interfaces and residue buried surface areas were determined using

Protein Interfaces, Surfaces and Assemblies (PISA) (*78*). The PyMOL Molecular Graphics System and GraphPad PRISM were used to produce graphical images and plots.

Statistical correlations between interface residue buried surface areas of shared MPER epitope residues between the VH7-4-1-using nAbs themselves and against other proximal MPER-targeting antibodies were determined by testing the null hypothesis that they were independent. The null hypothesis was that the correlations were zero (no correlation), and the alternative hypothesis was that correlations were non-zero. For the three VH7-4-1-using nAbs tested against each other, the null hypothesis was rejected by a significant *p*-value, supporting the possibility they had a positive correlation with each other. For the correlation of representative VH7-4-1 nAb DH1317.8 against DH570, m66, and 2F5, the results did not reject the null hypothesis, suggesting they had no correlation. Statistical tests and results for the analysis were generated in GraphPad PRISM using the Pearson correlation function.

Negative stain electron microscopy

For forming complexes, 1-5 µg JR-FL SOSIP.683 trimer was mixed with 6 molar concentration of Fab and incubated at 4 °C overnight. A portion of complex was then diluted to 20-50 µg/ml of SOSIP with buffer containing 20 mM HEPES, pH 7.4, 150 mM NaCl and 0.02 g/dL Ruthenium Red. A 5-µl drop of diluted sample was then applied to a glow-discharged, carbon-coated EM grid for 8-10 second, blotted, consecutively rinsed with 2 drops of dilute buffer containing 1 mM HEPES, pH 7.4 and 7.5 mM NaCl, and immediately blotted, stained with 2 g/dL uranyl formate for 1 min, blotted, and air-dried. Grids were examined on a Philips EM420 electron microscope operating at 120 kV and nominal magnification of 49,000x, and **~120** images for each sample were collected on a 76 Mpix CCD camera at a nominal calibration of 2.2 Å/pixel. Images were analyzed and 3D reconstructions calculated with Relion 3.0 (*79*). Data flow for symmetry expansion and focused 3D classification of the MPER Fabs is described in **Figure S9**.

Cryo-Electron microscopy

The trimer complex sample was deposited to glow-discharged QUANTIFOIL holey carbon grids (R1.2/1.3 Cu 300 mesh). After a 30 second incubation in 90-95% relative humidity, excess protein was blotted away with filter paper. The grid was plunge frozen in liquid ethane using an EM GP2 plunge freezer (Leica, Microsystems). Cryo-EM data were collected using a 300 kV FEI Titan Krios electron microscope (ThermoFisher) equipped with a K3 camera (Gatan) and GIF Quantum energy filter (20eV slit width) operating at 105Kx magnification with a pixel size of 1.08 Å with a defocus range between -1 and -3 µm. Gatan Latitude software was used to collect a total of 6,941 movies with a dose rate of 59.1 $e^-/Å^2$. All data processing steps were carried out in cryoSparc (https://www.nature.com/articles/nmeth.4169). Movie frames were aligned and dose weighted, followed by CTF estimation, particle picking, 2D classifications, 3D classifications using ab initio and heterogenous classifications, followed by 3D refinement.

References

1. B. F. Haynes, D. R. Burton, Developing an HIV vaccine. *Science* **355**, 1129-1130 (2017).
2. B. F. Haynes, D. R. Burton, J. R. Mascola, Multiple roles for HIV broadly neutralizing antibodies. *Sci Transl Med* **11**, (2019).
3. B. F. Haynes, L. Verkoczy, AIDS/HIV. Host controls of HIV neutralizing antibodies. *Science* **344**, 588-589 (2014).
4. B. F. Haynes *et al.*, HIV-Host Interactions: Implications for Vaccine Design. *Cell Host Microbe* **19**, 292-303 (2016).
5. M. A. Moody *et al.*, Immune perturbations in HIV-1-infected individuals who make broadly neutralizing antibodies. *Sci Immunol* **1**, aag0851 (2016).
6. P. Hraber *et al.*, Prevalence of broadly neutralizing antibody responses during chronic HIV-1 infection. *AIDS* **28**, 163-169 (2014).
7. E. Landais, P. L. Moore, Development of broadly neutralizing antibodies in HIV-1 infected elite neutralizers. *Retrovirology* **15**, 61 (2018).
8. S. M. Dennison *et al.*, Induction of antibodies in rhesus macaques that recognize a fusion-intermediate conformation of HIV-1 gp41. *PLoS One* **6**, e27824 (2011).
9. S. M. Alam *et al.*, Differential reactivity of germ line allelic variants of a broadly neutralizing HIV-1 antibody to a gp41 fusion intermediate conformation. *J Virol* **85**, 11725-11731 (2011).
10. S. M. Dennison *et al.*, Stable docking of neutralizing human immunodeficiency virus type 1 gp41 membrane-proximal external region monoclonal antibodies 2F5 and 4E10 is dependent on the membrane immersion depth of their epitope regions. *J Virol* **83**, 10211-10223 (2009).

11. B. F. Haynes *et al.*, Immune-correlates analysis of an HIV-1 vaccine efficacy trial. *N Engl J Med* **366**, 1275-1286 (2012).
12. S. Rerks-Ngarm *et al.*, Vaccination with ALVAC and AIDSVAX to prevent HIV-1 infection in Thailand. *N Engl J Med* **361**, 2209-2220 (2009).
13. B. F. Haynes *et al.*, Strategies for HIV-1 vaccines that induce broadly neutralizing antibodies. *Nat Rev Immunol*, (2022).
14. G. E. Gray *et al.*, Vaccine Efficacy of ALVAC-HIV and Bivalent Subtype C gp120-MF59 in Adults. *N Engl J Med* **384**, 1089-1100 (2021).
15. P. K. Ehrenberg *et al.*, A vaccine-induced gene expression signature correlates with protection against SIV and HIV in multiple trials. *Sci Transl Med* **11**, (2019).
16. D. Sok, D. R. Burton, Recent progress in broadly neutralizing antibodies to HIV. *Nat Immunol* **19**, 1179-1188 (2018).
17. K. Wiehe *et al.*, Functional Relevance of Improbable Antibody Mutations for HIV Broadly Neutralizing Antibody Development. *Cell Host Microbe* **23**, 759-765.e756 (2018).
18. M. Bonsignori *et al.*, Staged induction of HIV-1 glycan-dependent broadly neutralizing antibodies. *Sci Transl Med* **9**, (2017).
19. M. Bonsignori *et al.*, Maturation Pathway from Germline to Broad HIV-1 Neutralizer of a CD4-Mimic Antibody. *Cell*, (2016).
20. B. F. Haynes *et al.*, Cardiolipin polyspecific autoreactivity in two broadly neutralizing HIV-1 antibodies. *Science* **308**, 1906-1908 (2005).
21. B. F. Haynes, G. Kelsoe, S. C. Harrison, T. B. Kepler, B-cell-lineage immunogen design in vaccine development with HIV-1 as a case study. *Nat Biotechnol* **30**, 423-433 (2012).
22. T. Bradley *et al.*, Immune checkpoint modulation enhances HIV-1 antibody induction. *Nat Commun* **11**, 948 (2020).
23. L. Verkoczy *et al.*, Rescue of HIV-1 broad neutralizing antibody-expressing B cells in 2F5 VH x VL knockin mice reveals multiple tolerance controls. *J Immunol* **187**, 3785-3797 (2011).
24. L. Verkoczy *et al.*, Induction of HIV-1 broad neutralizing antibodies in 2F5 knock-in mice: selection against membrane proximal external region-associated autoreactivity limits T-dependent responses. *J Immunol* **191**, 2538-2550 (2013).
25. L. Verkoczy *et al.*, Autoreactivity in an HIV-1 broadly reactive neutralizing antibody variable region heavy chain induces immunologic tolerance. *Proc Natl Acad Sci U S A* **107**, 181-186 (2010).
26. G. E. Seabright, K. J. Doores, D. R. Burton, M. Crispin, Protein and Glycan Mimicry in HIV Vaccine Design. *J Mol Biol* **431**, 2223-2247 (2019).
27. C. Caillat, D. Guilligay, G. Sulbaran, W. Weissenhorn, Neutralizing Antibodies Targeting HIV-1 gp41. *Viruses* **12**, (2020).
28. G. Stiegler *et al.*, A potent cross-clade neutralizing human monoclonal antibody against a novel epitope on gp41 of human immunodeficiency virus type 1. *AIDS Res Hum Retroviruses* **17**, 1757-1765 (2001).
29. M. B. Zwick *et al.*, Broadly neutralizing antibodies targeted to the membrane-proximal external region of human immunodeficiency virus type 1 glycoprotein gp41. *J Virol* **75**, 10892-10905 (2001).
30. L. D. Williams *et al.*, Potent and broad HIV-neutralizing antibodies in memory B cells and plasma. *Sci Immunol* **2**, (2017).
31. J. Huang *et al.*, Broad and potent neutralization of HIV-1 by a gp41-specific human antibody. *Nature* **491**, 406-412 (2012).
32. Z. Zhu *et al.*, Cross-reactive HIV-1-neutralizing human monoclonal antibodies identified from a patient with 2F5-like antibodies. *J Virol* **85**, 11401-11408 (2011).
33. S. M. Alam *et al.*, The role of antibody polyspecificity and lipid reactivity in binding of broadly neutralizing anti-HIV-1 envelope human monoclonal antibodies 2F5 and 4E10 to

glycoprotein 41 membrane proximal envelope epitopes. *J Immunol* **178**, 4424-4435 (2007).

34. S. M. Alam *et al.*, Role of HIV membrane in neutralization by two broadly neutralizing antibodies. *Proc Natl Acad Sci U S A* **106**, 20234-20239 (2009).
35. A. Irimia, A. Sarkar, R. L. Stanfield, I. A. Wilson, Crystallographic Identification of Lipid as an Integral Component of the Epitope of HIV Broadly Neutralizing Antibody 4E10. *Immunity* **44**, 21-31 (2016).
36. Y. Chen *et al.*, Common tolerance mechanisms, but distinct cross-reactivities associated with gp41 and lipids, limit production of HIV-1 broad neutralizing antibodies 2F5 and 4E10. *J Immunol* **191**, 1260-1275 (2013).
37. R. Zhang *et al.*, Initiation of immune tolerance-controlled HIV gp41 neutralizing B cell lineages. *Sci Transl Med* **8**, 336ra362 (2016).
38. L. G. Perez, M. R. Costa, C. A. Todd, B. F. Haynes, D. C. Montefiori, Utilization of immunoglobulin G Fc receptors by human immunodeficiency virus type 1: a specific role for antibodies against the membrane-proximal external region of gp41. *J Virol* **83**, 7397-7410 (2009).
39. D. C. Montefiori *et al.*, The high-affinity immunoglobulin receptor FcγRI potentiates HIV-1 neutralization via antibodies against the gp41 N-heptad repeat. *Proc Natl Acad Sci U S A* **118**, (2021).
40. M. G. Pauthner *et al.*, Vaccine-Induced Protection from Homologous Tier 2 SHIV Challenge in Nonhuman Primates Depends on Serum-Neutralizing Antibody Titers. *Immunity* **50**, 241-252.e246 (2019).
41. K. O. Saunders *et al.*, Stabilized HIV-1 envelope immunization induces neutralizing antibodies to the CD4bs and protects macaques against mucosal infection. *Sci Transl Med* **14**, eabo5598 (2022).
42. A. Pegu *et al.*, A Meta-analysis of Passive Immunization Studies Shows that Serum-Neutralizing Antibody Titer Associates with Protection against SHIV Challenge. *Cell Host Microbe* **26**, 336-346.e333 (2019).
43. L. Corey *et al.*, Two Randomized Trials of Neutralizing Antibodies to Prevent HIV-1 Acquisition. *N Engl J Med* **384**, 1003-1014 (2021).
44. H. X. Liao *et al.*, Co-evolution of a broadly neutralizing HIV-1 antibody and founder virus. *Nature* **496**, 469-476 (2013).
45. K. O. Saunders *et al.*, Targeted selection of HIV-specific antibody mutations by engineering B cell maturation. *Science* **366**, (2019).
46. W. B. Williams *et al.*, Initiation of HIV neutralizing B cell lineages with sequential envelope immunizations. *Nat Commun* **8**, 1732 (2017).
47. K. O. Saunders *et al.*, Vaccine Induction of Heterologous Tier 2 HIV-1 Neutralizing Antibodies in Animal Models. *Cell Rep* **21**, 3681-3690 (2017).
48. D. J. Leggat *et al.*, Vaccination induces HIV broadly neutralizing antibody precursors in humans. *Science* **378**, eadd6502 (2022).
49. K. Xu *et al.*, Epitope-based vaccine design yields fusion peptide-directed antibodies that neutralize diverse strains of HIV-1. *Nat Med* **24**, 857-867 (2018).
50. L. Ou *et al.*, Preclinical Development of a Fusion Peptide Conjugate as an HIV Vaccine Immunogen. *Sci Rep* **10**, 3032 (2020).
51. N. Erdmann *et al.*, A Gp41 Liposome Vaccine Elicits HIV-1 MPER-Specific Antibody Responses in Healthy Humans. *In preparation*, (2023).
52. T. Muster *et al.*, Cross-neutralizing activity against divergent human immunodeficiency virus type 1 isolates induced by the gp41 sequence ELDKWAS. *J Virol* **68**, 4031-4034 (1994).
53. J. Finney *et al.*, Cross-Reactivity to Kynureninase Tolerizes B Cells That Express the HIV-1 Broadly Neutralizing Antibody 2F5. *J Immunol* **203**, 3268-3281 (2019).

54. G. Yang *et al.*, Identification of autoantigens recognized by the 2F5 and 4E10 broadly neutralizing HIV-1 antibodies. *J Exp Med* **210**, 241-256 (2013).
55. M. Ohlin, Poorly Expressed Alleles of Several Human Immunoglobulin Heavy Chain Variable Genes are Common in the Human Population. *Front Immunol* **11**, 603980 (2020).
56. W. B. Williams *et al.*, Fab-dimerized glycan-reactive antibodies are a structural category of natural antibodies. *Cell*, (2021).
57. A. Ramesh *et al.*, Structure and Diversity of the Rhesus Macaque Immunoglobulin Loci through Multiple. *Front Immunol* **8**, 1407 (2017).
58. T. B. Kepler *et al.*, Reconstructing a B-Cell Clonal Lineage. II. Mutation, Selection, and Affinity Maturation. *Front Immunol* **5**, 170 (2014).
59. S. M. Alam *et al.*, Antigenicity and Immunogenicity of HIV-1 Envelope Trimers Complexed to a Small-Molecule Viral Entry Inhibitor. *J Virol* **94**, (2020).
60. G. Ofek *et al.*, Structural basis for HIV-1 neutralization by 2F5-like antibodies m66 and m66.6. *J Virol* **88**, 2426-2441 (2014).
61. G. Ofek *et al.*, Structure and mechanistic analysis of the anti-human immunodeficiency virus type 1 antibody 2F5 in complex with its gp41 epitope. *J Virol* **78**, 10724-10737 (2004).
62. M. Medina-Ramírez *et al.*, Design and crystal structure of a native-like HIV-1 envelope trimer that engages multiple broadly neutralizing antibody precursors in vivo. *J Exp Med* **214**, 2573-2590 (2017).
63. M. Tian *et al.*, Induction of HIV Neutralizing Antibody Lineages in Mice with Diverse Precursor Repertoires. *Cell* **166**, 1471-1484.e1418 (2016).
64. H. X. Liao *et al.*, High-throughput isolation of immunoglobulin genes from single human B cells and expression as monoclonal antibodies. *J Virol Methods* **158**, 171-179 (2009).
65. L. Morris *et al.*, Isolation of a human anti-HIV gp41 membrane proximal region neutralizing antibody by antigen-specific single B cell sorting. *PLoS One* **6**, e23532 (2011).
66. E. J. Platt, K. Wehrly, S. E. Kuhmann, B. Chesebro, D. Kabat, Effects of CCR5 and CD4 cell surface concentrations on infections by macrophagetropic isolates of human immunodeficiency virus type 1. *J Virol* **72**, 2855-2864 (1998).
67. D. C. Montefiori, Measuring HIV neutralization in a luciferase reporter gene assay. *Methods Mol Biol* **485**, 395-405 (2009).
68. C. A. Bricault *et al.*, HIV-1 Neutralizing Antibody Signatures and Application to Epitope-Targeted Vaccine Design. *Cell Host Microbe* **25**, 59-72.e58 (2019).
69. P. Virtanen *et al.*, SciPy 1.0: fundamental algorithms for scientific computing in Python. *Nat Methods* **17**, 261-272 (2020).
70. C. Snider, S. Jayasinghe, K. Hristova, S. H. White, MPEx: a tool for exploring membrane proteins. *Protein Sci* **18**, 2624-2628 (2009).
71. W. C. Wimley, S. H. White, Experimentally determined hydrophobicity scale for proteins at membrane interfaces. *Nat Struct Biol* **3**, 842-848 (1996).
72. J. Dunbar, C. M. Deane, ANARCI: antigen receptor numbering and receptor classification. *Bioinformatics* **32**, 298-300 (2016).
73. Z. Otwinowski, W. Minor, Processing of X-ray diffraction data collected in oscillation mode. *Methods Enzymol* **276**, 307-326 (1997).
74. W. Kabsch, Xds. *Acta Crystallogr D Biol Crystallogr* **66**, 125-132 (2010).
75. P. D. Adams *et al.*, PHENIX: a comprehensive Python-based system for macromolecular structure solution. *Acta Crystallogr D Biol Crystallogr* **66**, 213-221 (2010).
76. P. Emsley, K. Cowtan, Coot: model-building tools for molecular graphics. *Acta Crystallogr D Biol Crystallogr* **60**, 2126-2132 (2004).

77. P. D. Adams *et al.*, PHENIX: building new software for automated crystallographic structure determination. *Acta Crystallogr D Biol Crystallogr* **58**, 1948-1954 (2002).
78. E. Krissinel, K. Henrick, Inference of macromolecular assemblies from crystalline state. *J Mol Biol* **372**, 774-797 (2007).
79. J. Zivanov *et al.*, New tools for automated high-resolution cryo-EM structure determination in RELION-3. *Elife* **7**, (2018).

Figure 1

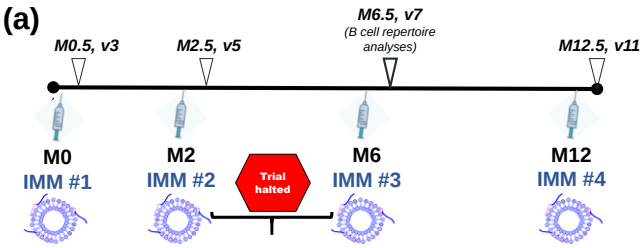

(b)

Study group	Number of immunizations/ Vaccine recipients		Number of immunizations/ Placebo recipients	
	IMMs = 2	IMMs = 3	IMMs = 2	IMMs = 3
500 mcg	5	3	1	1
2000 mcg	15	2	3	0
Totals	20	5	4	1

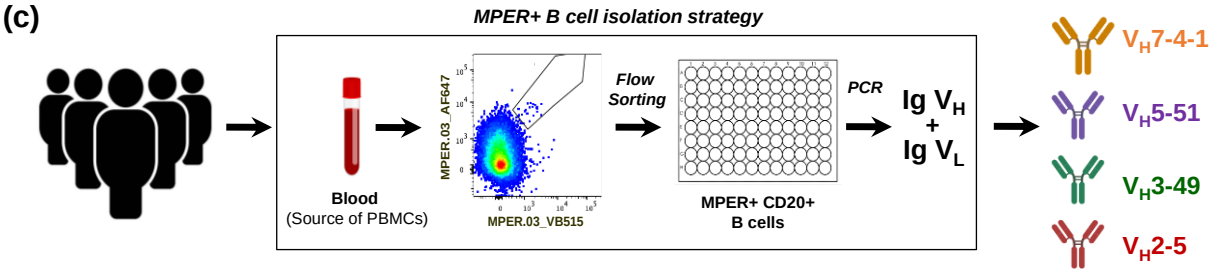

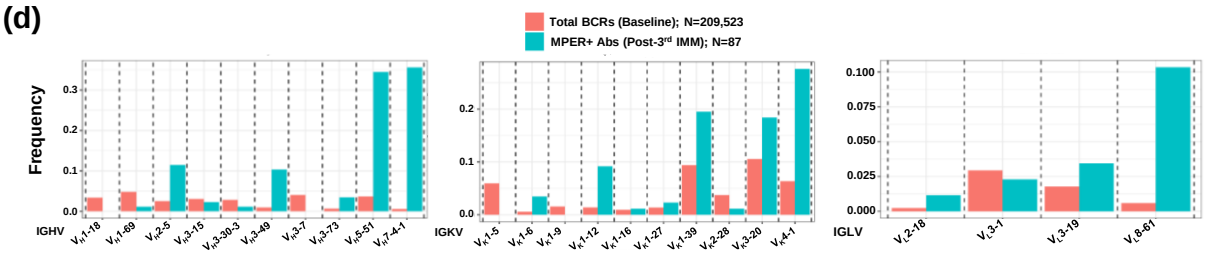

(e)

Predominant VH gene usage	Abs (no.)	MPERΔ	Cross-reactivity to non-HIV antigens		
			KYNU	Cardiolipin	Autoantigens
V_H2-5	10	10/10 (100%)	10/10 (100%)	5/10 (50%)	7/10 (70%)
V_H3-49	9	9/9 (100%)	0/9 (0%)	0/9 (0%)	0/9 (0%)
V_H5-51	30	28/30 (93%)	3/30 (10%)	4/24 (17%)	9/30 (30%)
V_H7-4-1	31	24/31 (77%)	1/31 (3%)	5/27 (18.5%)	14/31 (45%)

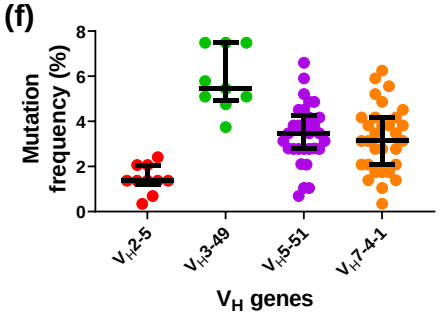

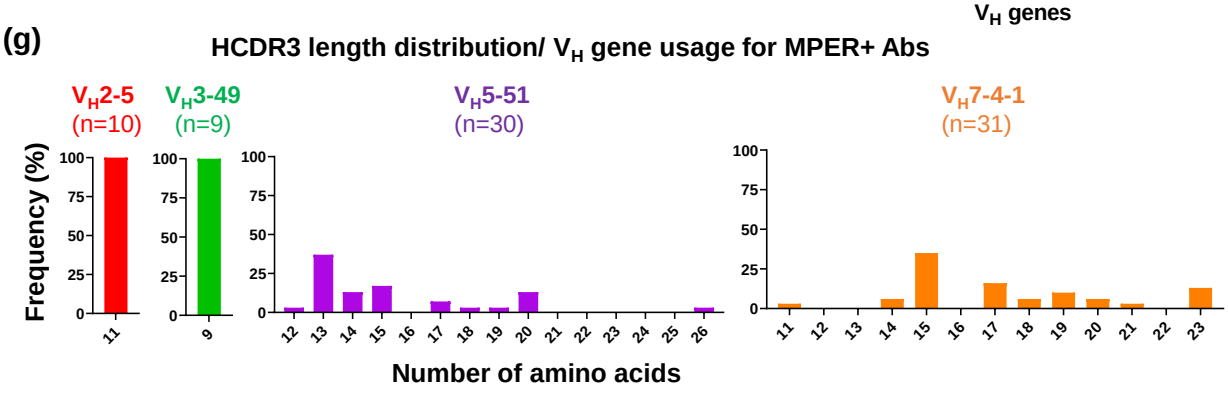

Figure 1 legend is on the next page.

Figure 1. HVTN133 Clinical Trial Elicited a Polyclonal MPER+ Ab Response. **(a)** Immunization (IMM) schedule for HVTN133. The timeline for IMMs in months (M) is indicated. Peripheral blood was collected from the participants at two weeks after each IMM for characterization of vaccine-induced responses. B cell repertoire analyses reported in this study was done on peripheral blood cells (PBMCs) collected 2 weeks post-3rd IMM. The trial was halted after one vaccine recipient developed an anaphylactic reaction 4 hours post-3rd IMM. All participants received the 2nd IMM, but only five vaccine recipients received the 3rd IMM. **(b)** Vaccine recipients were divided into two groups based on Alum dosing of 500 or 2000 mcg. There were four placebo recipients across both groups. **(c)** Schema for B cell repertoire analysis performed on PBMCs from 5 HVTN133 vaccinees who received three IMMs. Boxed area: MPER+ B cells were flow sorted and Ig VH and VL genes recovered from each single sorted B cells to generate recombinant Abs for binding and functional screens. The top 4 V_H genes used by MPER+ Abs were V_H2-5, V_H3-49, V_H5-51 and V_H7-4-1, characteristic of a polyclonal response. **(d)** Frequency of immunoglobulin (Ig) genes used by MPER+ Abs isolated from blood in HVTN133 vaccine recipients post-3rd IMM. For comparison, we studied antigen-unbiased B cell receptor repertoire pre-IMM in all five vaccinees. Data shown reflect individual Ig gene usages and not paired heavy and light chain gene pairs. From our reference dataset of antigen-naïve total BCR repertoires, we report only the Ig genes used by MPER+ Abs in the HVTN133 vaccinees. The total number of Abs studied per group is listed in the figure key. Not shown: immunogenetics of two MPER+ Abs at baseline from 2/5 vaccinees studied (133-30 and 133-23). **(e)** Tally of Abs isolated post-3rd immunization that were categorized based on predominant V_H gene used by MPER+ Abs, and frequency of MPER+ Abs tested for different binding specificities; MPERΔ bnAb precursor phenotype and cross-reactivity to non-HIV antigens (Kynu, Cardiolipin and autoantigens). All Abs were tested for MPER binding phenotypes and Kynu-reactivity, but only a subset of Abs were tested for cross-reactivity with cardiolipin and autoantigens. **(f)** Mutation frequency of the predominant V_H genes used by MPER+ Abs. Each dot represents a single Ab. Error bars represent the median and interquartile range (GraphPad Prism, v9.0). **(g)** CDR3 length distributions of predominant V_H genes used by MPER+ Abs. HCDR3 length is reported in amino acids (x-axis) and the frequency (%) of Abs with the indicated amino acid length is shown on the y-axis.

Figure 2

(a) *MPER bnAb maturation pathway*

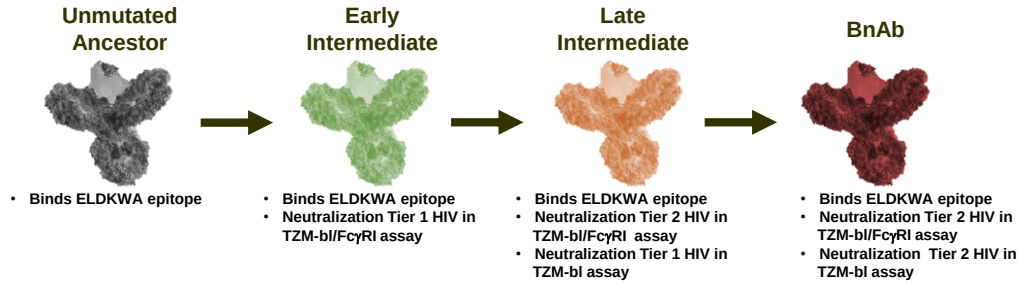

(b) *Screen for MPER NAbs (HVTN133)*

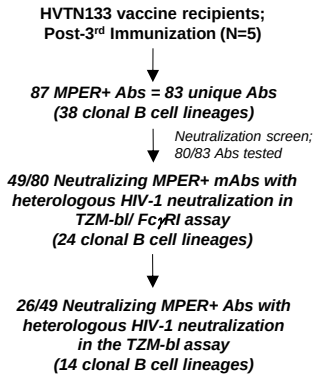

(d) *Neutralization breadth; DH1317.4 Ab*

TZM-bl neutralization of V_H7-4-1-using DH1317.4 bnAb	IC50	ID80
Geomean, µg/ml	13.1	18.9
# of HIV-1 strains neutralized	29	12
Breadth, Multiclade (N=197)	15%	6.1%
Breadth, Clade B (N=72)	35% (25/72)	12.5% (9/72)
Breadth, Clade B Tier 2/ 3 & AMP Trial strains (N=64)	31% (20/64)	11% (7/64)

(e) *DH1317 neutralization curves, Clade B HIV-1*

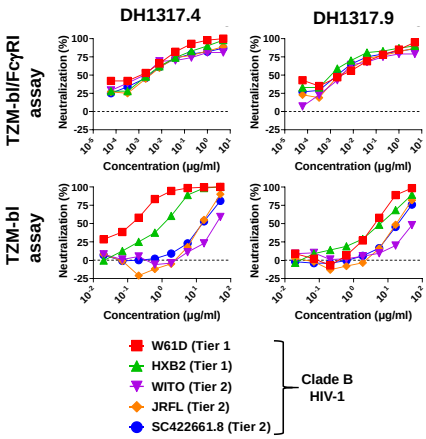

Figure 2C is on the next page.

Figure 2

(c) *Clade B, HIV-1 neutralization; MPER+ nAbs (n=49)*

IC50, µg/mL	<0.1	0.1-1	1-10	10-50	>50

Ab ID	IGHV gene	Neutralization titers, IC50 µg/ml) - Tier 1 and 2 Clade B HIV-1 strains											
		TZM-bl/FcγRI						TZM-bl					
		MuLV	W61D	HXB2	WITO	JRFL	SC422661.8	MuLV	W61D	HXB2	WITO	JRFL	SC422661.8
		n/a	Tier 1	Tier 1	Tier 2	Tier 2	Tier 2	TZM-bl	TZM-bl	TZM-bl	TZM-bl	TZM-bl	TZM-bl
DH1355	IGHV1-69	>50	0.85	0.91	>50	>50	>50	>50	18	14	>50	>50	>50
DH1316.3	IGHV2-5	>50	9.0	7.2	>50	>50	>50	>50	>50	>50	>50	>50	>50
DH1316.8	IGHV2-5	>50	4.0	0.64	failed	>50	>50	>50	>50	>50	>50	>50	>50
DH1318.2	IGHV3-49	>50	0.10	<0.02	1.1	0.09	0.15	>50	4.4	30	>50	>50	>50
DH1318.3_7	IGHV3-49	>50	0.04	<0.02	<0.02	1.1	0.43	>50	3.9	19	>50	>50	>50
DH1318.4	IGHV3-49	>50	28	2.5	>50	36	>50	>50	>50	>50	>50	>50	>50
DH1318.5	IGHV3-49	>50	3.9	<0.02	0.26	1.1	0.40	>50	24	>50	>50	>50	>50
DH1318.6	IGHV3-49	>50	0.38	<0.02	0.04	0.26	0.12	>50	5.5	15	>50	>50	>50
DH1318.8	IGHV3-49	>50	30	25.3	>50	1.6	>50	>50	>50	>50	>50	>50	>50
DH1318.9	IGHV3-49	>50	2.2	<0.02	1.7	0.91	3.0	>50	19	>50	>50	>50	>50
DH1353	IGHV3-73	>50	<0.02	<0.02	>50	<0.02	0.02	>50	>50	>50	>50	>50	>50
DH1321.1	IGHV5-51	>50	2.6	<0.02	23	0.02	0.11	>50	>50	>50	>50	>50	>50
DH1321.2	IGHV5-51	>50	>50	0.08	>50	0.13	0.16	>50	>50	>50	>50	>50	>50
DH1321.4	IGHV5-51	>50	>50	failed	>50	0.71	>50	>50	>50	>50	>50	>50	>50
DH1352.1	IGHV5-51	>50	>50	<0.02	37	0.24	14	>50	>50	>50	>50	>50	>50
DH1352.2	IGHV5-51	>50	>50	<0.02	>50	0.13	2.7	>50	>50	>50	>50	>50	>50
DH1354	IGHV5-51	>50	<0.02	<0.02	<0.02	<0.02	0.03	>50	15	31	>50	>50	>50
DH1360	IGHV5-51	>50	<0.02	<0.02	0.004	0.08	>50	>50	46.2	>50	>50	>50	>50
DH1362.2	IGHV5-51	>50	>50	<0.02	3.3	0.12	0.11	>50	>50	>50	>50	>50	>50
DH1362.3	IGHV5-51	>50	<0.02	<0.02	<0.02	<0.02	<0.02	>50	6.4	27	>50	>50	>50
DH1362.4	IGHV5-51	>50	>50	<0.02	>50	>50	>50	>50	>50	>50	>50	>50	>50
DH1363.2	IGHV5-51	>50	>50	<0.02	0.15	0.24	0.96	>50	>50	>50	>50	>50	>50
DH1420	IGHV5-51	>50	<0.02	<0.02	0.05	0.04	0.03	>50	36	>50	>50	>50	>50
DH1421	IGHV5-51	>50	0.23	<0.02	0.18	0.05	<0.02	>50	>50	>50	>50	>50	>50
DH1423	IGHV5-51	>50	<0.02	<0.02	0.07	0.06	0.05	>50	3.5	25	>50	>50	>50
DH1317.1	IGHV7-4-1	>50	<0.02	<0.02	<0.02	<0.02	<0.02	>50	0.24	2.5	>50	20	28
DH1317.2	IGHV7-4-1	>50	<0.02	<0.02	<0.02	<0.02	<0.02	>50	0.26	2.3	>50	26	50
DH1317.3	IGHV7-4-1	>50	<0.02	<0.02	<0.02	<0.02	<0.02	>50	0.45	4.3	>50	21	23
DH1317.4	IGHV7-4-1	>50	<0.02	<0.02	<0.02	<0.02	<0.02	>50	0.14	1.2	41	13	16
DH1317.6	IGHV7-4-1	>50	<0.02	<0.02	<0.02	<0.02	<0.02	>50	1.0	3.7	>50	23	35
DH1317.7	IGHV7-4-1	>50	<0.02	<0.02	<0.02	<0.02	<0.02	>50	0.46	5.1	>50	22	41
DH1317.8	IGHV7-4-1	>50	<0.02	<0.02	0.10	<0.02	<0.02	>50	1.7	5.1	>50	>50	>50
DH1317.9	IGHV7-4-1	>50	<0.02	<0.02	<0.02	<0.02	<0.02	>50	3.0	3.4	46	12	11
DH1319.1	IGHV7-4-1	>50	<0.02	<0.02	>50	<0.02	<0.02	>50	6.5	37	>50	>50	>50
DH1319.2	IGHV7-4-1	>50	<0.02	<0.02	>50	0.06	0.05	>50	>50	>50	>50	>50	>50
DH1322.1	IGHV7-4-1	>50	0.65	2.1	>50	0.18	1.5	>50	34	>50	>50	>50	>50
DH1346	IGHV7-4-1	>50	1.6	<0.02	>50	<0.02	0.03	>50	39	16	>50	>50	>50
DH1347.1	IGHV7-4-1	>50	>50	<0.02	>50	0.97	>50	>50	>50	>50	>50	>50	>50
DH1347.2	IGHV7-4-1	>50	0.03	<0.02	>50	<0.02	<0.02	>50	16	>50	>50	>50	>50
DH1347.3	IGHV7-4-1	>50	2.2	<0.02	>50	<0.02	0.17	>50	15	31	>50	>50	>50
DH1349.1_2	IGHV7-4-1	>50	0.47	0.17	>50	1.8	>50	>50	>50	>50	>50	>50	>50
DH1349.3	IGHV7-4-1	>50	0.07	<0.02	>50	<0.02	0.07	>50	>50	>50	>50	>50	>50
DH1350	IGHV7-4-1	>50	<0.02	<0.02	>50	<0.02	0.06	>50	>50	>50	>50	>50	>50
DH1351.1	IGHV7-4-1	>50	>50	0.11	>50	>50	>50	>50	>50	>50	>50	>50	>50
DH1351.2	IGHV7-4-1	>50	32	<0.02	>50	<0.02	0.76	>50	>50	27	>50	>50	>50
DH1361.1	IGHV7-4-1	>50	1.3	1.1	>50	0.31	failed	>50	>50	>50	>50	>50	>50
DH1361.2	IGHV7-4-1	>50	>50	0.70	>50	3.1	>50	>50	>50	>50	>50	>50	>50
DH1413	IGHV7-4-1	>50	>50	>50	>50	43	>50	>50	>50	>50	>50	>50	>50
DH1425	IGHV7-4-1	>50	<0.02	<0.02	>50	<0.02	<0.02	>50	>50	20	>50	37	>50

Figure 2 legend is on the next page.

Figure 2. Neutralization Breadth Profile of Vaccine-induced DH1317 BnAb. (a) Schematic outlining maturation pathway for MPER bnAbs. **(b)** Flowchart summarizing the neutralization screens for MPER+ recombinant Abs isolated from HVTN133 vaccine recipients post-3rd immunization. Eighty unique Abs representative of 83 total MPER+ Abs were tested for neutralization. Three additional MPER+ Abs were not tested for neutralization due to low Ab yields following 293i cell transfections. **(c)** Neutralization profile of 49/80 MPER+ Abs that neutralized tier 1 or 2 clade B HIV-1 strains in TZM-bl/FcgRI or TZM-bl assays. Neutralization titers were measured in IC50 (µg/ml). **(d)** Summary of neutralization breadth for one representative member (DH1317.4) of a V_H7-4-1-using DH1317 clonal lineage of Abs that demonstrated neutralization of heterologous tier 1 and 2 HIV-1 strains in panel C. **(e)** Neutralization curves against tier 1 and 2 clade B HIV-1 strains for representative DH1317 lineage Abs; DH1317.4 and DH1317.9. Neutralization was performed in the TZM-bl and TZM-bl/FcgRI assays. Data shown are from a single or duplicate experiments; the mean titers are shown for results from duplicate experiments.

Figure 3

(a)

Neutralization profile			V_H gene	HCDR3 length (aa)	mAb ID	SP62 peptides: WT	E662A	L663A	D664A	K665A	W666A	S668A	L669A
TZM-bl/ FcγRI (Tier 1/2)	TZM-bl (Tier 1)	TZM-bl (Tier 2)											
+	+	+	V_H2-5	24	2F5	12.7	12.5	12.7	0.5	8.7	0	12.6	12.2
+	+	+	V_H5-51	21	M66.6	13.5	14.0	0.4	6.1	0.3	0.9	13.3	13.7
			V_H2-5	11	DH1316.8	18.4	18.3	16.9	0.9	16.9	16.8	18.1	18.1
+	+	-	V_H3-49	9	DH1318.2	16.2	16.3	14.7	1.2	15.7	16.7	16.8	15.9
+	-	-	V_H5-51	15	DH1321.1	16.6	16.7	6.3	14.0	0.8	13.3	16.4	16.1
+	+	-	V_H7-4-1	23	DH1322.1	14.7	14.1	14.0	6.5	15.2	13.3	15.3	15.1
+	+	-	V_H7-4-1	20	DH1346	15.8	15.9	15.5	15.4	14.4	15.2	15.5	15.6
+	+	-	V_H7-4-1	18	DH1319.1	16.3	16.5	16.5	6.4	15.7	16.5	15.9	15.8
+	+	-	V_H7-4-1	15	DH1317.8	16.1	16.1	16.4	3.9	15.5	16.1	15.6	15.3
+	+	+	V_H7-4-1	15	DH1317.9	17.0	17.2	17.1	2.0	16.9	16.9	16.8	17.0
+	+	+	V_H7-4-1	15	DH1317.4	15.5	16.7	16.1	5.9	15.9	16.0	14.7	14.8

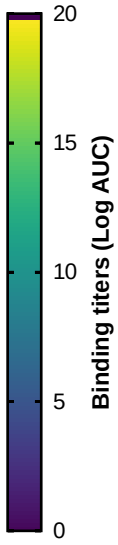

(b) *DH1317 neutralization of multiclade HIV in TZM-bl/FcγRI assay*

IC50, µg/mL	<0.1	0.1-1	1-10	10-50	>50

Virus Name	Clade	Neutralization titers in TZM-bl/FcγRI assay: DH1317.9 IC50	DH1317.9 IC80	DH1317.4 IC50	DH1317.4 IC80	M66.6 IC50	M66.6 IC80	2F5 IC50	2F5 IC80
HIV H704_2684_181_RE_p001s	B	<0.02	0.6	<0.02	0.8	>50	>50	>50	>50
H704_1535_030sN	B	<0.02	>50	0.1	>50	>50	>50	>50	>50
H704_0026_231_RE_pbsga001_s	B	>50	>50	>50	>50	<0.02	0.07	<0.02	0.06
V704_0372_250_RE_pblib001_s	B	<0.02	0.09	<0.02	0.05	<0.02	0.04	<0.02	<0.02
H704_0855_080_EsN	B	>50	>50	>50	>50	<0.02	0.9	<0.02	0.07
6644.v2.c33	C	>50	>50	>50	>50	>50	>50	>50	>50
TV1.21	C	>50	>50	>50	>50	<0.02	<0.02	<0.02	0.04
3168.v4.c10	C	>50	>50	>50	>50	<0.02	>50	<0.02	11
ZM197M.PB7	C	<0.02	2.6	<0.02	>50	<0.02	0.1	<0.02	>50
CAP206.1.B5	C	>50	>50	>50	>50	>50	>50	>50	>50
CNE5	AE	>50	>50	>50	>50	<0.02	0.2	<0.02	0.3
CNE59	AE	>50	>50	>50	>50	<0.02	<0.02	<0.02	<0.02
T242-14	AG	>50	>50	>50	>50	<0.02	0.5	<0.02	0.05
T257-31	AG	<0.02	>50	<0.02	>50	<0.02	0.6	<0.02	0.3
T253-11	AG	<0.02	33	<0.02	14	<0.02	0.1	<0.02	0.05
Q23.17	A	>50	>50	>50	>50	<0.02	0.1	<0.02	0.1
MS208.A1	A	0.09	>50	0.03	>50	<0.02	<0.02	<0.02	<0.02
92UG024.2	D	>50	>50	>50	>50	<0.02	<0.02	<0.02	0.03
T247-23	D	>50	>50	>50	>50	<0.02	<0.02	<0.02	0.02
SVA-MLV	negative	>50	>50	>50	>50	>50	>50	>50	>50

Figure 3C is on the next page.

Figure 3

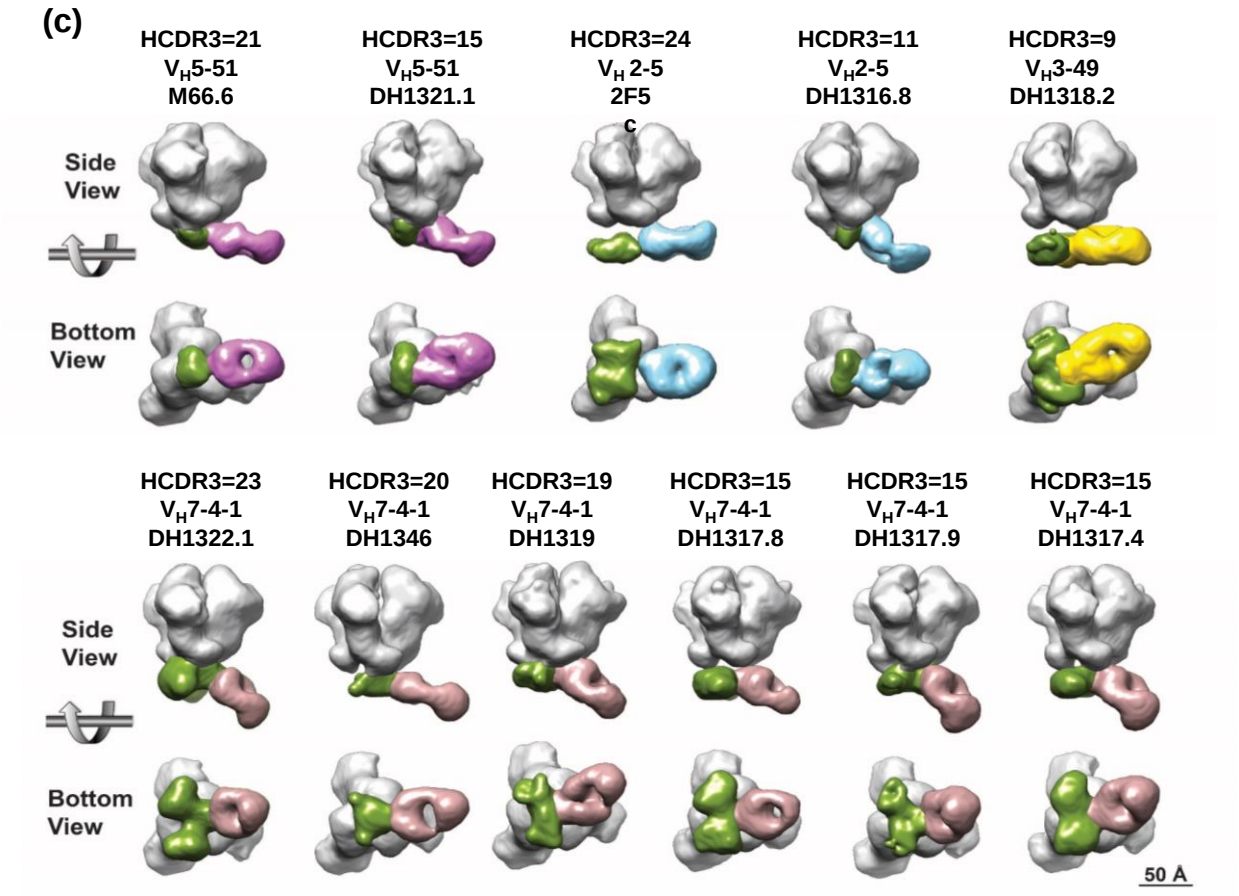

Figure 3. MPER+ NAbs Mapped to Proximal BNAb Epitopes. (a) *(Left)* A summary of neutralization profile and heavy chain gene used by the MPER+ nAbs. *(Right)* Mapping of MPER+ nAbs to proximal MPER bnAb epitope in SP62 peptides. Binding was measured in ELISA and reported as Log AUC as shown in the heatmap. Binding sensitivity or epitope mapping to a specific residue in SP62 tested were based on ≥50% reduction in binding to single alanine-scanned mutant peptides compared to the wild-type. **(b)** Neutralization titers of DH1317.4, DH1317.9 and MPER proximal bnAbs M66.6 and 2F5 tested against a panel of clade B HIV-1 strains from the AMP trial and non-clade B HIV-1 strains. Neutralization titers shown were measured in the TZM-bl/FcgRI assay and titers reported as IC50 and IC80 (µg/ml). DH1317.4 and DH1317.9 did not neutralize these viruses with titers <50µg/ml in the TZM-bl assay (see Figure S3). **(c)** NSEM maps for 11 MPER-directed Abs shown in side and bottom views. The Env trimer, excluding the MPER domain is colored gray, the MPER region with partial Fab density is colored green, and the MPER Fabs are colored according to their heavy chain gene as follows: V_H5-51 = pink; V_H2-5 = sky blue; V_H3-49 = gold, and V_H7-4-1 = brown.

Figure 4

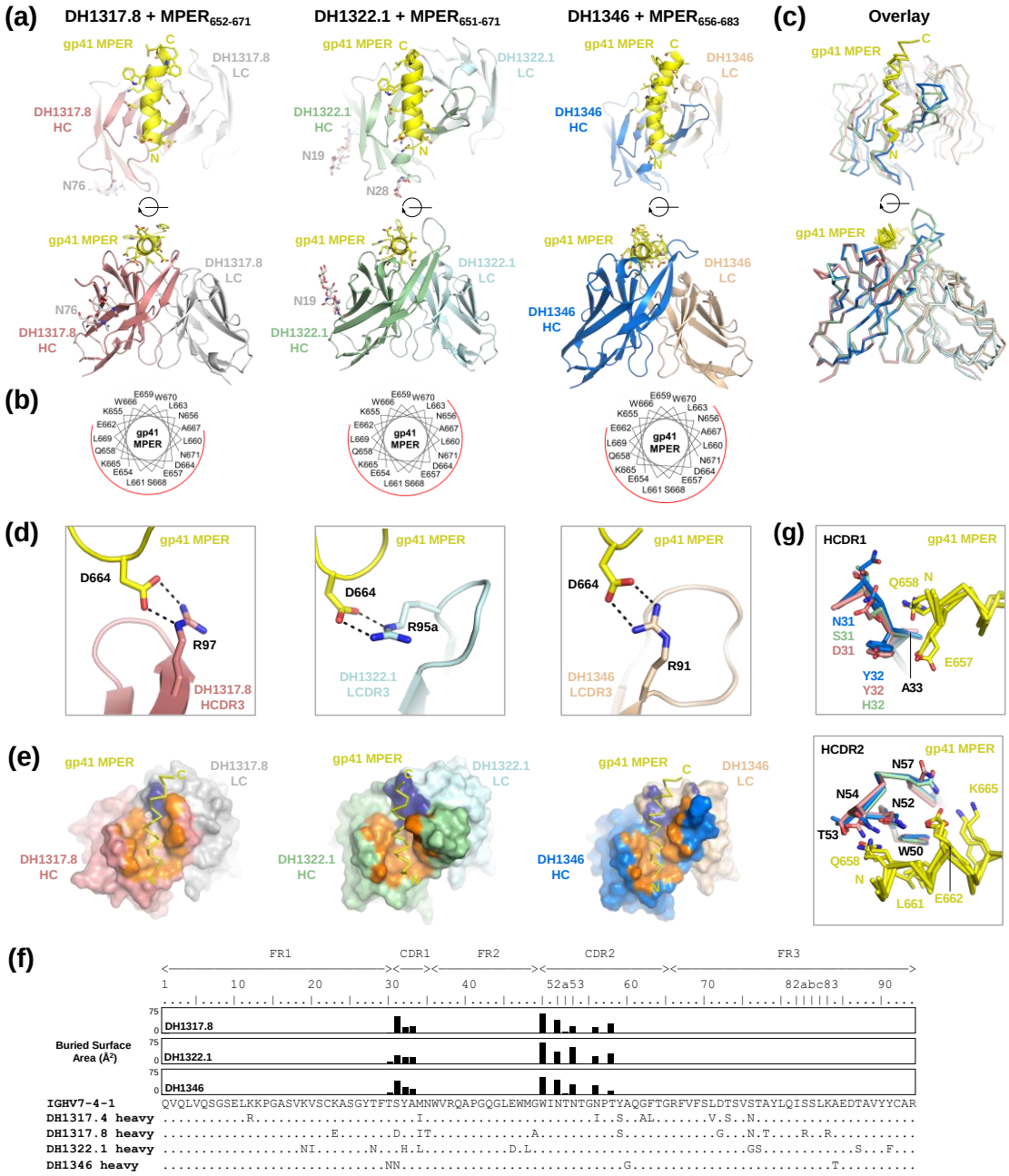

Figure 4 legend is on the next page.

Figure 4. Structural Analysis of the Polyclonal V_H7-4-1 Ab Response to the MPER Peptide-Liposome in Vaccinee 133-23. (a) Structures of nAbs DH1317.8, DH1322.1, and DH1346 in complex with MPER peptides, with variable regions shown in two orientations. **(b)** Helical wheel representations of MPER with nAb contacting faces shown in red. **(c).** Overlay of Ab complexes based on alignment of common V_H7-4-1 regions, shown in same orientations and colors as in **panel a**. **(d)** Salt bridge interactions between MPER residue D664 and nAbs DH1317.8, DH1322.1, and DH1346. **(e)** Paratope interfaces on DH1317.8, DH1322.1, and DH1346 mapped orange on heavy chains and dark blue on light chains, shown in same orientation as in **panel a** (top). **(f)** Sequence alignment of the heavy chain regions of DH1317.4, DH1317.8, DH1322.1, and DH1346 against V_H7-4-1 germline gene, with interface residue BSAs plotted as bars above. **(g)** V_H7-4-1-encoded HCDR1 and HCDR2 loops in DH1317.8, DH1322.1, and DH1346 adopt similar conformations and interact with the same set of MPER residues, underpinning common modes of Ab recognition.

Figure 5

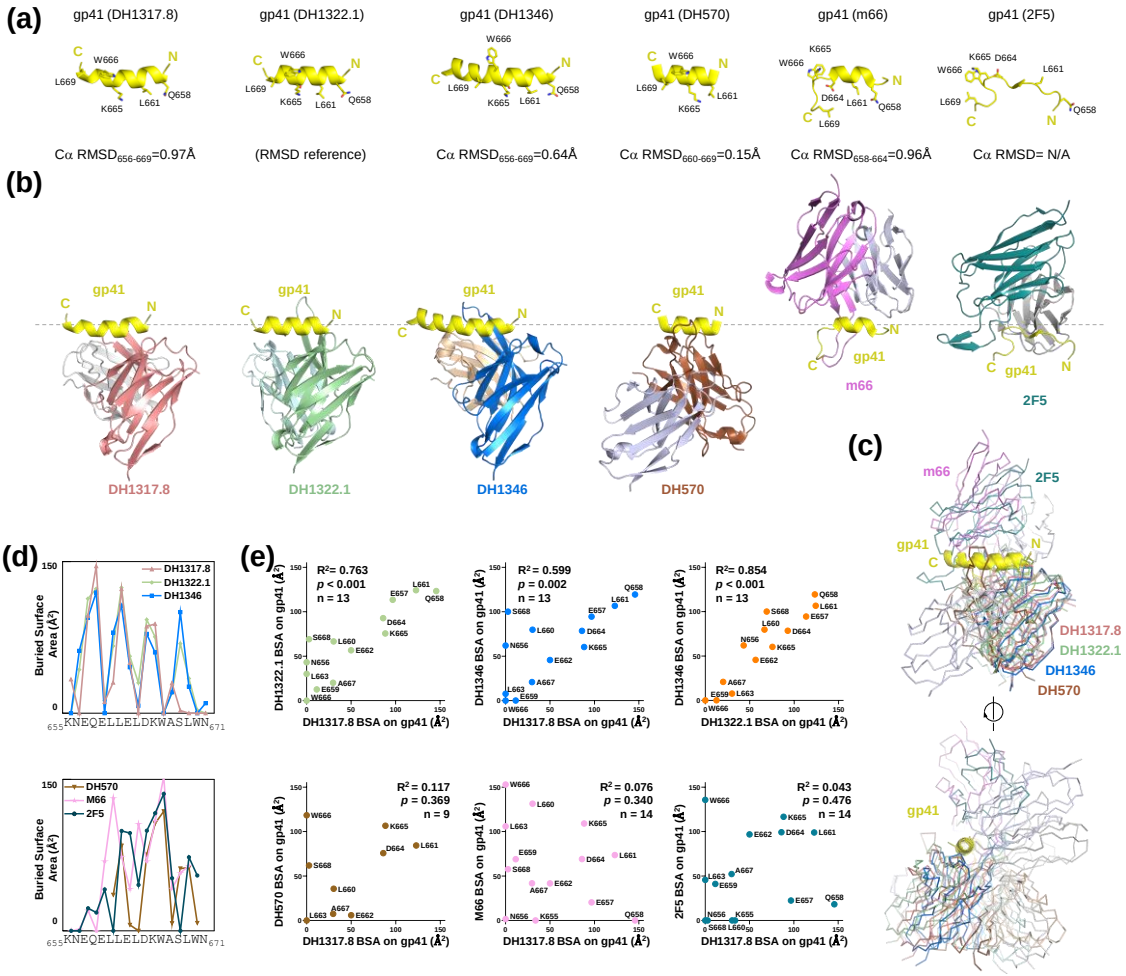

Figure 5. Structural Comparison of Ab Recognition of Proximal Gp41 MPER. (a) DH1317.8, DH1322.1, DH1346, DH570 (5DD0), m66 (4NRX), and 2F5 (1TJI)-bound conformations of proximal gp41 MPER (yellow), oriented based on Ca alignments to reference DH1322.1-bound MPER. R.m.s.d. values shown for residue ranges used in the alignments. The epitope of 2F5 is shown based on alignment to residues 664-666 of m66-bound MPER. **(b)** Ab variable region structures bound to MPER, orientated based on bound MPER peptides as shown in **panel a**. **(c)** Overlay of MPER-bound Ab variable region structures shown in same orientations and colors as in **panel B** (top), and rotated ~90° (bottom). **(d)** Plots of interface residue buried surface areas (BSA) along proximal MPER for DH1317.8, DH1322.1, and DH1346 (top) and DH570, m66, and 2F5 (bottom). **(e)** Pairwise correlation analysis of buried surface areas (BSA) of shared MPER interface residues between V_H7-4-1-using nAbs themselves (upper panels) and with reference Abs DH570, m66, and 2F5 (lower panels).

Figure 6

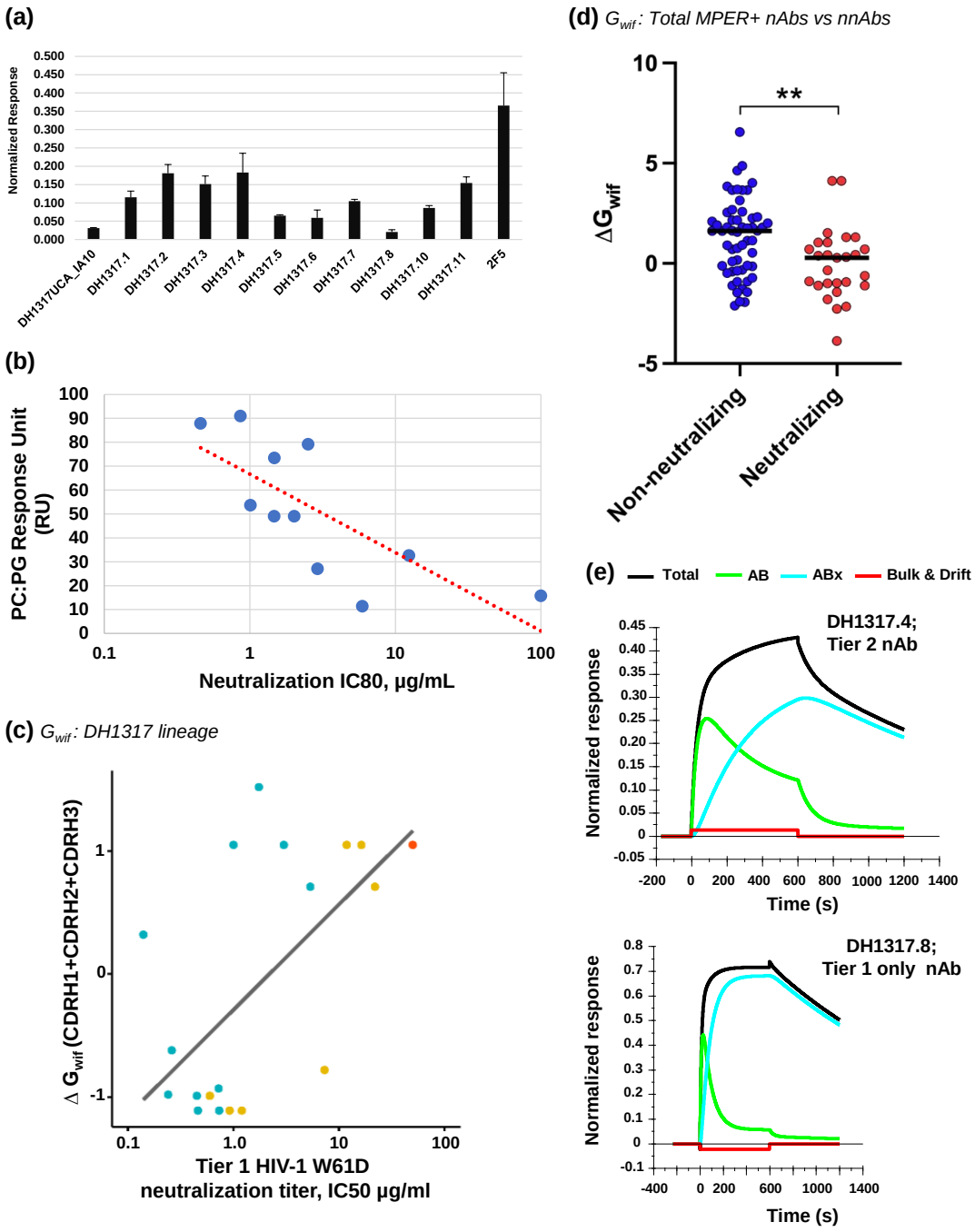

Figure 6 legend is on next page.

Figure 6. Lipid Reactivity Profiles of DH1317 Lineage Abs. (a) Binding of each indicated Ab at 100µg/mL to POPC:DOPG (25:75) liposomes were measured by surface plasmon resonance (SPR) and plotted data show binding responses in RU normalized to control surface (lipophilic linker) and capture level of liposomes. Values and error bars represent the average and standard deviation of three measurements. **(b)** Plot of phosphatidylglycerol lipid (PC:PG) binding response unit (RU) versus W61D pseudovirus neutralization IC80 values of each of the DH1317 lineage Abs. DH1317 UCA IC80 of >50 µg/mL is plotted with a given value of 100 µg/mL. Phosphatidylgycerol lipid containing binary liposomes were prepared using phospholipids POPC and DOPG as described in methods and binding response to DH1317 Abs were measured using SPR analysis. The plotted PC:PG binding responses are mean values of three independent experiments. Kendall's Tau correlation coefficient =0.6363, P=0.0054 for both IC80 and IC50 values. **(c)** Computed lipid insertion propensity scores ΔG_{wif} of HCDR1, 2 and 3 (summed) vs. W61D neutralization IC50 (µg/mL). Computed lipid insertion propensity scores ΔG_{wif} (kcal/mol) for HCDR1, 2 and 3 (summed) is positively correlated with log W61D neutralization potency for DH1317 clonal members (R = 0.61, P = 0.0043, Pearson correlation). Lower ΔG_{wif} scores correspond to more favorable lipid insertion propensity. Isolated members of the DH1317 clone are shown in blue, inferred intermediate Abs in yellow, and inferred UCA in red. **(d)** Computed lipid insertion propensity scores ΔG_{wif} (kcal/mol) for HCDR1, 2 and 3 (summed) are significantly higher (less favorable for lipid insertion) in W61D nnAbs (blue) than nAbs (red). ** $p<0.01$; Mann-Whitney test. The ΔG_{wif} score is based on free energy of binding, where negative free energy is more favorable. **(e)** Biolayer interferometry (BLI) binding of DH1317.4 heterologous tier 2 nAb (top) or DH1317.8 (bottom) tier 1 only nAb Fabs to MPER liposomes fitted to the 2-step conformational change model. SPR binding curve (black) in each panel is overlayed with resolved component curves representing the encounter (first step, green) and the docked complexes (2nd step, blue).